Biological transformation of Arctic dissolved organic matter in a NE Greenland fjord

Maria Lund Paulsen ©,*[1] Oliver Müller,[1] Aud Larsen,[1,2] Eva Friis Møller ©,[3,4] Mathias Middelboe,[5] Mikael K. Sejr,[4] Colin Stedmon[6]

[1]Department of Biology, University of Bergen, Bergen, Norway
[2]NORCE Norwegian Research Center AS, Bergen, Norway
[3]Department of Bioscience, Aarhus University, Roskilde, Denmark
[4]Arctic Research Centre, Aarhus University, Aarhus C, Denmark
[5]Marine Biological Section, University of Copenhagen, Helsingør, Denmark
[6]National Institute of Aquatic Resources, Technical University of Denmark, Kgs. Lyngby, Denmark

Abstract

Arctic waters are often enriched with terrestrial dissolved organic matter (DOM) characterized by having elevated visible wavelength fluorescence (commonly termed humic-like). Here, we have identified the sources of fluorescent DOM (FDOM) in a high Arctic fjord (Young Sound, NE Greenland) influenced by glacial meltwater. The biological transformation of FDOM was further investigated using plankton community size-fractionation experiments. The intensity of ultraviolet fluorescence (commonly termed amino acid-like) was highly variable and positively correlated to bacterial production and mesozooplankton grazing. The overall distribution of visible FDOM in the fjord was hydrographically driven by the high-signal intrusion of Arctic terrestrial DOM from shelf waters and dilution with glacial runoff in the surface waters. However, the high-intensity visible FDOM that accumulated in subsurface waters in summer was not solely linked to allochthonous sources. Our data indicate that microbial activity, in particular, protist bacterivory, to be a source. A decrease in visible FDOM in subsurface waters was concurrent with an increase in bacterial abundance, indicating an active bacterial uptake or modification of this DOM fraction. This was confirmed by net-loss of visible FDOM in experiments during summer when bacterial activity was high. The degradation of visible FDOM appeared to be associated with bacteria belonging to the order Alteromonadales mainly the genus *Glaciecola* and the SAR92 clade. The findings provide new insight into the character of Arctic terrestrial DOM and the biological production and degradation of both visible and UV wavelength organic matter in the coastal Arctic.

Microorganisms produce, transform, and consume dissolved organic matter (DOM) and as a result, all aquatic environments contain a complex mixture of organic molecules that vary greatly in chemical characteristics and size. This results in a considerable analytical challenge for resolving the production, turnover, and fate of carbon, nitrogen, and phosphorus bound as organic matter. The most common approach to quantify DOM is to measure its carbon content (dissolved organic carbon [DOC]), however, this provides no information on DOM characteristics, which ultimately impacts its fate. Other

measures such as bioavailable DOC (BDOC) (Søndergaard and Middelboe 1995), and optical properties of the organic matter (Stedmon and Nelson 2015), offer insight into the DOM character. Fluorescent DOM (FDOM) signal can be separated into underlying components which group into broad visible wavelength "humic-like" fluorescence (henceforth termed visible fluorescence) and ultraviolet wavelength fluorescence (henceforth termed UV fluorescence) which is typical for simpler structures such free or combined amino acids or benzoic acid derivatives (Wünsch et al. 2015).

Arctic waters are characterized by having elevated visible fluorescence and this is linked to the high-terrestrial input of organic matter (Amon et al. 2003; Walker et al. 2013), which have been used to trace large-scale water mass distribution of Arctic water (Amon et al. 2003; Gonçalves-Araujo et al. 2016). The rapid warming of the Arctic cryosphere is increasing riverine discharge and thus the land to ocean transport of organic carbon (Holmes et al. 2008; Feng et al. 2013). In the glacial

*Correspondence: maria.l.paulsen@uib.no

Additional Supporting Information may be found in the online version of this article.

fjords of Greenland, the rate of ice loss from the Greenland Ice Sheet has doubled in the last decade (Kjeldsen et al. 2015). Glacial meltwater from the ice sheet contains a significant fraction of bioavailable DOM (Lawson et al. 2014; Paulsen et al. 2017), which potentially constitutes an important carbon source for coastal and marine food webs. This is particularly relevant in low productive Arctic systems characterized by a short ice-free summer, stratification, and low-light conditions due to riverine freshwater and inorganic particle input. Increases in stratification limit inorganic nutrient replenishment from deeper waters and thus we can expect that local primary production is more dependent on allochthonous inputs and local mineralization. Young Sound in North East Greenland (Fig. 1) is typical for such an Arctic system. It is influenced by meltwater from the Greenland Ice Sheet via land-terminating glaciers, while the marine end-member of the fjord originates from the East Greenland Current stemming from the Arctic. Local conditions are changing and this is evident as the average salinity from 2003 to 2015, has decreased in Young Sound by 0.12 per year indicating an increased influence of freshwater (Sejr et al. 2017).

Young Sound is considered to be low productive (annual pelagic primary productivity of 10.3 g C m^{-2} yr^{-1}; Rysgaard et al. 1999), due to the short sea ice-free season allowing for only 30% of the yearly photosynthetically active radiation (PAR) flux to reach the water column. Further, the silty glacial runoff drastically reduces the euphotic depth. The effects of the glacial runoff on the distribution of micro- and mesozooplankton (Arendt et al. 2016; Middelbo et al. 2018), marine ecosystem productivity (Meire et al. 2017), colored DOM

absorption (Murray et al. 2015), and the carbon availability for bacteria (Paulsen et al. 2017) have previously been described for Young Sound. Small phytoplankton (< 2 μm) dominate the murky inner fjord and contribute on average 89% of chlorophyll *a* (Chl *a*) compared to 59% at the mouth of the fjord. At the same time, copepod grazing is considerably less in the inner fjord (Middelbo et al. 2018), while protist grazing is enhanced (Arendt et al. 2016). Copepods and protists generally dominate the grazer biomass in Young Sound, although the pelagic gastropod *Limacina helicina* is abundant particularly in autumn (Middelbo et al. 2018).

The three major sources of organic carbon in Young Sound are (1) the local phytoplankton production, (2) runoff from land-terminating glaciers and lowland rivers, and (3) inflow from the East Greenland Current waters on the shelf. The fraction of bioavailable DOC (%BDOC) is highest in the glacial runoff (30–35%) and lowest in the subsurface fjord water (5–7%) (Paulsen et al. 2017). However, as DOC concentration in the glacial runoff is low, absolute BDOC concentrations for both are similar (15 ± 8 μM) (Paulsen et al. 2017). BDOC is difficult logistically to measure at high temporal and spatial resolution. Further, BDOC measurements do not reflect the degradation potential by the representative in situ bacterial communities when carried out in long-term (weeks to months) bottle experiments. FDOM components, instead, can be measured at high resolution and related to: changes in biological activity in the fjord; the in situ bacterial community composition; and changes occurring in short-term (days) incubations.

While FDOM has been used as a water mass tracer, little is known about how the biological processes in marine waters
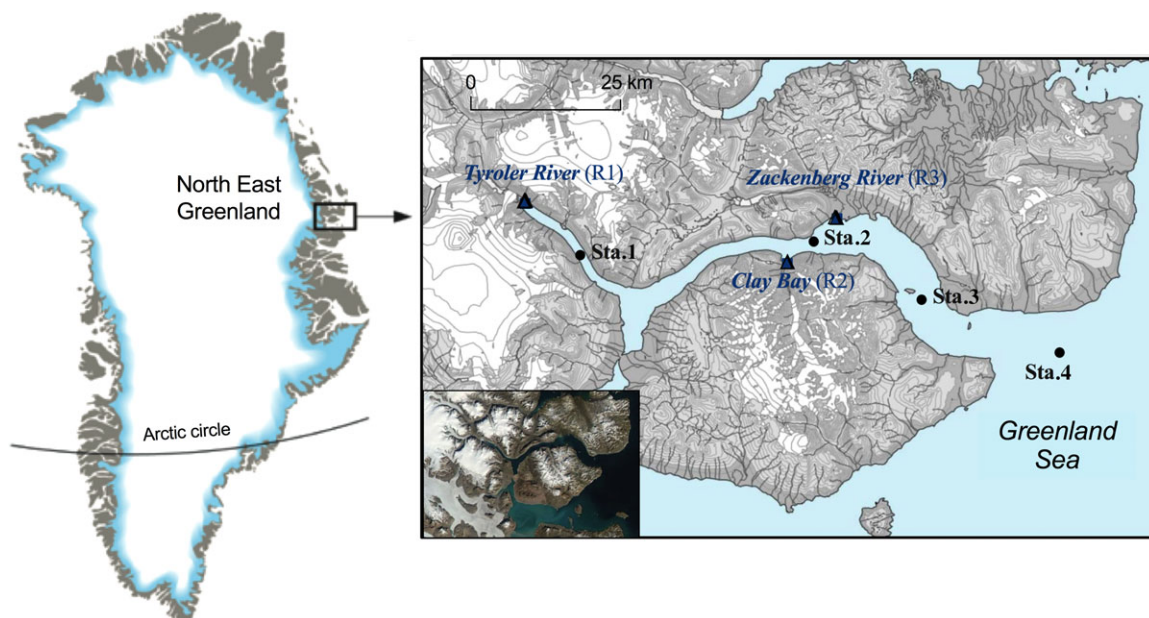

Fig. 1. Study sites in North East Greenland. Circles indicate the four sampling stations in Young Sound (Sta. 1–4) and triangles the three sampled rivers (R1–R3). Satellite image in the bottom left corner illustrates the glacial cover at its minimum in August (available at http://ocean.dmi.dk/arctic/daneborg.uk.php).

may transform the FDOM signature (i.e., cause breakage or production of fluorescent molecular structures) and thus alter its terrestrial character in Arctic waters. Several recent studies have aimed to link the spatial and vertical distribution of FDOM components to biological standing-stock parameters such as bacterial abundance (Catalá et al. 2016) or Chl *a* fluorescence (Lønborg et al. 2014; Gonçalves-Araujo et al. 2016; Sa and Kim 2017), but not to biological processes and activity. Bacteria are often considered to be the sole decomposers of DOM and can consume UV FDOM and produce visible FDOM (Guillemette and del Giorgio 2012; Lønborg et al. 2014). The latter is therefore considered to be less bioavailable and correlates negatively to bacterial growth efficiency and BDOC (Asmala et al. 2013). The accumulation of visible FDOM in the deep ocean is attributed to aphotic bacterial transformation of organic matter (Yamashita and Tanoue 2008; Jørgensen et al. 2011; Aparicio et al. 2015). However, DOM is produced at all levels of the food web (Jiao et al. 2010; Lønborg et al. 2013; Stedmon and Cory 2014) and there is also evidence that protist grazing of bacteria produces high-molecular weight DOM with a visible FDOM signature (Nagata and Kirchman 1992; Baña et al. 2014).

Here, we evaluate the sources of FDOM in the Young Sound fjord system and further study the biological transformation of DOM in short-term (days) incubation experiments designed to contain a representative in situ microbial community composition. While considering the FDOM signature from mesozooplankton grazers (copepods and pteropods) and different size classes of phytoplankton, the main focus is on the effect that bacteria and heterotrophic nanoflagellate (HNF) grazing activity have on the FDOM signal. Three central questions were addressed: (1) Can FDOM be used as a tracer in the fjord to distinguish between different DOM sources, (2) What imprint does the open water productivity period leave on the FDOM signal, and (3) Is the fjord microbial community capable of modifying visible- and UV FDOM?

Material and methods

Study site and sampling

The study was conducted in the Tyroler fjord-Young Sound system, Northeast Greenland (74.2–74.3°N, 19.7–21.9°W) (Fig. 1). The system is 90 km long, 2–7 km wide, and covers an area of 390 km^2, with a maximum depth of 360 m. One 45-m sill is situated in the inner part of the system at the mouth of Tyroler fjord, and a second sill separates Young Sound from the East Greenland shelf waters (Fig. 2). Sampling was conducted at four stations located along the freshwater gradient from the inner fjord to the shelf (Sta. 1–4), and in the three major rivers (R1–R3) (Fig. 1). The fjord stations 1, 2, 3, and 4 are located according to stations monitored yearly by the Greenland Ecosystem Monitoring (GEM) MarinBasis Zackenberg program named Tyro 05, YS 3.18, Standard St. and GH 05, respectively. The fjord is influenced by runoff from June to September with an accumulated amount of ca. 0.9–1.4 km^3 yr^{-1} (Bendtsen et al. 2014). Land-terminating glaciers contribute on average 50–80% of the runoff, mainly in the inner part of the fjord (Citterio et al. 2017).

A Seabird SBE 19+ conductivity, temperature and depth (CTD) profiler was deployed at every sampling occasion and recorded vertical profiles of temperature (°C), salinity (practical salinity unit), oxygen (μmol kg^{-1}), Chl *a* fluorescence (flu$_{chl}$, relative; no units), turbidity (FTU), and PAR (μmol m^{-2} s^{-1}). Discrete water samples were taken at six depths (1 m, 10 m, 20 m, 30 m, 40 m, and 100 m) and additionally at the Chl *a* maximum/maxima with a 12 bottle, 1.2-liter Niskin mini-rosette. Location of the deep chlorophyll max (DCM) was determined just prior to every sampling occasion using a Satlantic Free-falling Optical Profiler. Each month a longitudinal transect with CTD stations every 5 km (25 CTD in total) were performed to obtain high-resolution coverage of the fjord hydrography (Fig. 2). Three of the major rivers discharging into the fjord were sampled as long as the water was flowing (the last sampling was on 10th September). The meltwater in the Tyroler river (R1) and Clay Bay river (R2) flows from glaciers through rocky sediment basins with very little vegetation and a distance of ca. 0.5 km and 2 km before they reach the fjord. Zackenberg river (R3) is different from the two others as the water has a longer residence time in two lakes and flow through the vegetated Zackenberg Valley before entering the fjord. As a result, DOC concentration in R3 is approximately 50% higher than R1 and R2 (Paulsen et al. 2017). A model study estimated the residence time of river water in the fjord to be about 2 weeks in July and up to a month in August (Bendtsen et al. 2014).

Water samples were kept in the dark in 10-liter opaque high-density polyethylene (HDPE) plastic containers and transported back to the Daneborg Marine Station (near Sta. 3) for further analysis. Chl *a* was analyzed according to Jespersen and Christoffersen (1987). Samples for DOC and total nitrogen (TN) concentrations were collected in 30 mL acid-washed HDPE bottles and stored at −20°C until analysis. Concentrations were determined by high-temperature combustion (720°C) using a Shimadzu TOC-V CPH-TN carbon and nitrogen analyser. Samples were acidified to pH 2 using hydrochloric acid. The instrument was calibrated using acetanilide (Cauwet 1999) and carbon determination was referenced to the community deep-sea reference (Hansell laboratory, Miami). Bacterial production (BP; μg C L^{-1} d^{-1}) was estimated from the incorporation of ^{3}H-thymidine in 10 mL samples in triplicate (Riemann et al. 1982). The specific BP (μg C L^{-1} d^{-1} cell^{-1}) was calculated as BP/bacterial abundance (cells L^{-1}). Oxidized nitrogen (NO$_2^-$ + NO$_3^-$), phosphate (PO$_4^{3-}$), and silicic acid (H$_4$SiO$_4$) were measured on a Smartchem200 (by AMS Alliance) autoanalyser following procedures as outlined in Wood et al. (1967) for NO$_3^-$ + NO$_2^-$, Murphy and Riley (1962) for PO$_4^{3-}$, Holmes et al. (1999) for NH$_4^+$, and Koroleff (1983) for the determination of H$_4$SiO$_4$. Water for DNA and RNA extraction was collected from the rivers and at
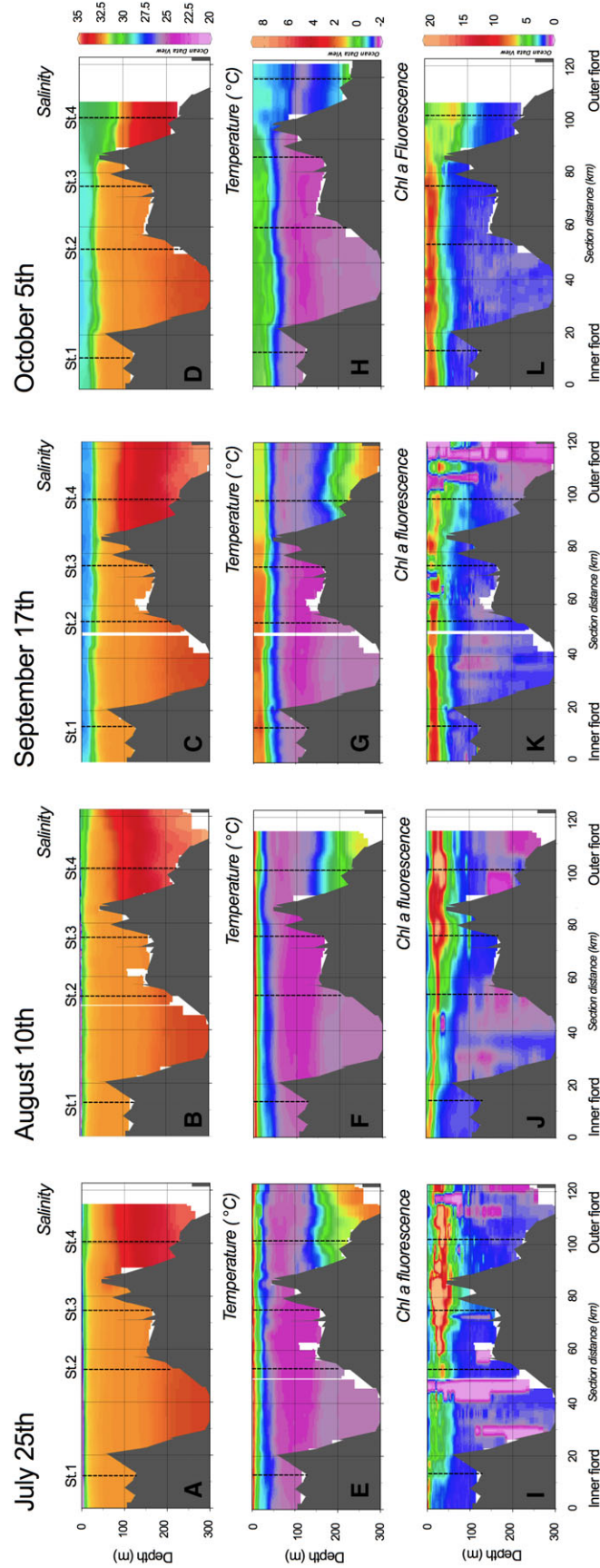
Fig. 2. Monthly fjord transects of salinity (**A–D**), temperature (**E–H**), Chl *a*-fluorescence (**I–L**) in Young Sound covering 25 CTD stations from the inner fjord (0 km) to the Greenland Sea. Dashed lines mark the four main stations. Plots were drawn using weighted-average gridding in Ocean Data View (Schlitzer 2016).

1 m and the DCM in the fjord, and water for size-fractionated Chl a and microsized protists were collected only at 1 m and the DCM in the fjord.

Dissolved organic matter fluorescence

Samples for DOM fluorescence from the fjord and experiments were filtered through 0.2 μm syringe filters (Acrodisc® ion chromatography) into acid cleaned and precombusted amber glass bottles and kept at 4°C until measured within 2 months. The logistics of sampling in North East Greenland across four expeditions hindered sample measurements on site and the measurements can potentially be influenced by microbial regrowth and organic matter degradation during storage despite 0.2 μm filtration. Seven samples were checked for bacterial regrowth during storage by 3 months and results showed a regrowth from < 200 cells mL^{-1} to 11.000 $\pm$ 7.500 cells mL^{-1}. No optimal sample storage procedure exists for FDOM, as the addition of preservatives and freezing can influence fluorescence more than sterile filtration alone (Schneider-Zapp et al. 2013). Samples were acclimated to room temperature before measurement on a Horiba Aqualog spectrofluorometer within 2 months. The instrument measured fluorescence intensity across emission wavelengths 300–600 nm at excitation wavelengths from 250 nm to 450 nm in a 1 cm quartz cuvette. Excitation-emission matrix (EEM) were merged into a three-dimensional matrix and analyzed via the multivariate data analysis technique parallel factor analysis (PARAFAC) (Murphy et al. 2013). FDOM signal was split into five components (Fig. 3) and they are named according to the wavelength at their emission maximum, and the "Coble's peaks" from Coble (1996) that each component resemble is displayed. Three components had emission maxima at visible wavelengths (C_{417}, C_{498}, C_{405}) and two at UV wavelengths (C_{340}, C_{310}). The fluorescence intensities reported here are at the excitation and emission maximum in Raman units, nm^{-1} (Lawaetz and Stedmon 2009).

To better reveal how DOM properties varied between different sources, samples were grouped by each river, and the water types defined as "river plume" ($S < 25$), "fjord surface waters" ($S = 25–32.5$ and $T > -1$°C), "subsurface waters" ($S < 32.5$ and $T < -1$°C), and "coastal shelf waters" ($S > 32.5$) as in Paulsen et al. (2017). The fluorescence intensity of the five components was averaged within each water type for each season (Fig. 4). The high salinity "coastal shelf water" was encountered only at Sta. 4, at 100 m (Fig. 2) at few sampling occasions, and FDOM was only sampled from this water type on three occasions. Therefore, our FDOM description of this end member is likely weaker than for the rivers.

Enumeration of microorganisms

The abundance of bacteria, heterotrophic HNFs, and small phytoplankton were determined on an Attune® Acoustic
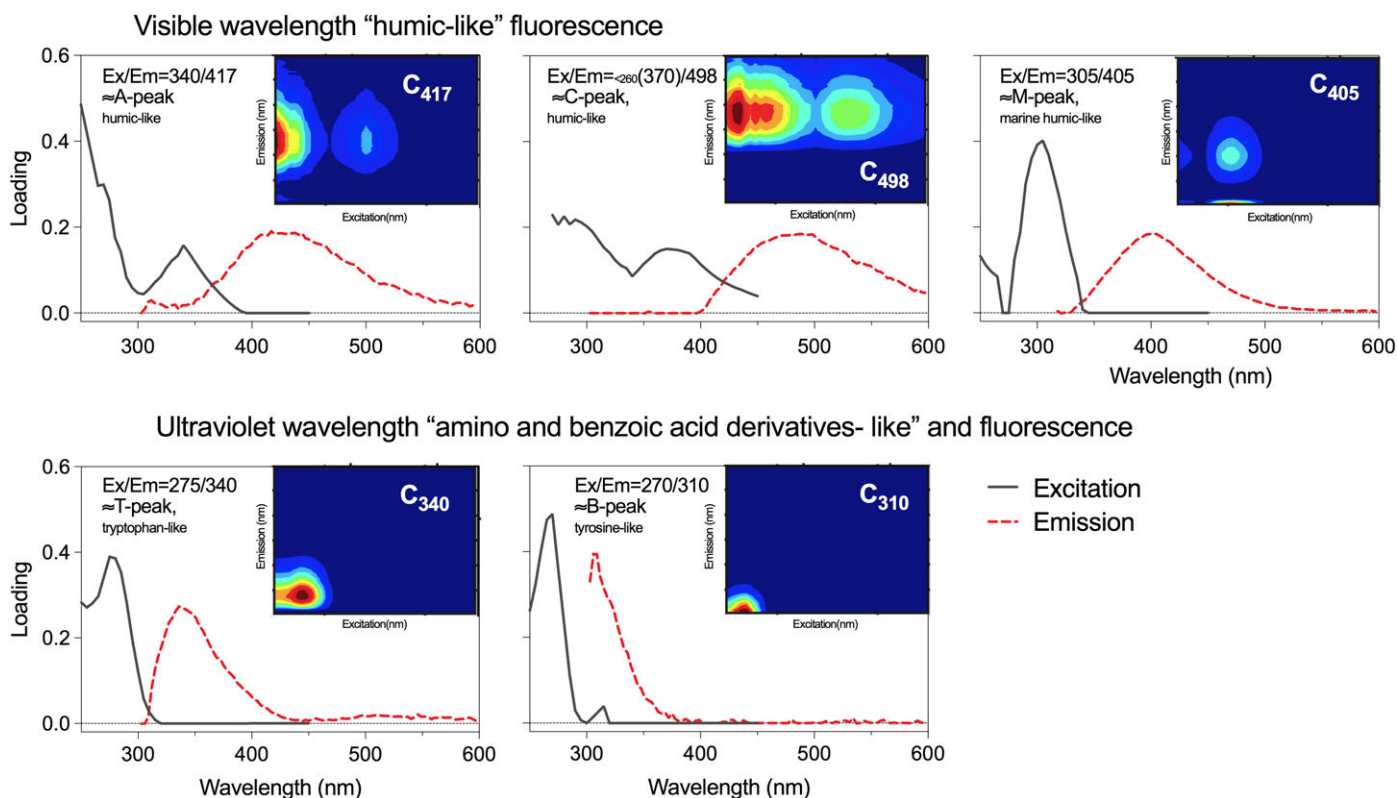

Fig. 3. The excitation (solid line) and emission (red dashed line) of the five FDOM components isolated by PARAFAC. The fluorescence maximum is shown as well as the "cer peaks" that each component resembles (Coble 1996). The three-dimensional fluorescence contour plots with emission on the y-axis (300–600 nm) and excitation on the x-axis (250–450 nm).

Focusing Flow Cytometer (Applied Biosystems by Life Technologies) with a syringe-based fluidic system and a 20 mW 488 nm (blue) laser (Paulsen et al. 2016). Samples for heterotrophic bacteria and HNFs were fixed with glutaraldehyde (0.5% final concentration) and kept dark at 4°C until analysis within 12 h. Phytoplankton samples were enumerated from fresh samples and the populations of pico- and nanosized phytoplankton were grouped based on their pigmentation on biplots of green vs. red fluorescence as in Paulsen et al. (2016). Samples for heterotrophic prokaryotes (hereafter bacteria) and HNF were stained with SYBR Green I (Molecular Probes, Eugene, Oregon, U.S.A.) for minimum 1 h. Bacteria were analyzed at a low-flow rate (25 μL min^{-1}) following the protocol of Marie et al. (1999). HNF were measured at a high-flow rate according to Zubkov et al. (2007) and subdivided into two different size groups of ca. 3–5 μm diameter (hereafter small HNF) and ca. 5–10 μm diameter (hereafter large HNF) by filtering parallel samples through 3 μm, 5 μm, and 10 μm polycarbonate filters and counting the filtrate and adjusting gates. The ratio of small HNF to bacteria is used here as an indicator of bacterial grazing pressure as in other studies (Sanders et al. 1992). Samples for the larger microsized protists (ciliates, heterotrophic dinoflagellates, and microphytoplankton) were fixed in acid Lugol's solution (2% final concentration) and stored cold and dark until analyses. Fifty milliliters were examined after 24 h sedimentation in Utermöhl chambers. The protists were enumerated and identified to species/morphotype level using an inverted microscope (magnification: ×200–400). While only heterotrophic dinoflagellates were enumerated by microscope, chloroplast 16S ribosomal ribonucleic acid (rRNA) gene analysis additionally detected autotrophic dinoflagellates.

DNA and RNA extraction, 16S rRNA sequencing, and data analysis

Samples for molecular analysis were collected by filtering onto 0.22 μm Sterivex filters (2 L filtered from environmental samples and 4 L from experiments). DNA and RNA were extracted simultaneously from the filters using the AllPrep DNA/RNA Mini Kit (Qiagen, Hilden, Germany). We used DNA for the analysis of the community composition in experimental samples and RNA for the analysis of the in situ fjord and river samples. RNA was treated with the DNA-free DNA Removal kit (Invitrogen, California, U.S.A.), and reverse transcribed using the SuperScript III First-Strand Synthesis System for reverse transcription polymerase chain reaction (RT-PCR) (Invitrogen). Amplification of complementary DNA (cDNA) and DNA was performed using a two-step nested PCR approach with primers 519F and 806R targeting both the archaeal and the bacterial 16S rRNA gene V4 hypervariable region. Details regarding extraction, amplification and amplicon library preparation can be found in Wilson et al. (2017). Libraries were sequenced at the Norwegian Sequencing Centre (Oslo, Norway) using their MiSeq platform (MiSeq Reagent Kit v2, Illumina, California, U.S.A.). Sequencing data are available

at "The European Bioinformatics Institute" under study accession number **PRJEB16067** (http://www.ebi.ac.uk).

Paired-end sequences were processed using different bioinformatic tools incorporated on a qiime-processing platform (Caporaso et al. 2011) as described in Paulsen et al. (2016). FASTQ files were quality end-trimmed, merged and prokaryotic operational taxonomic units (OTUs) were selected at a sequence similarity threshold of 97%. Taxonomy was assigned using the Greengenes reference database (DeSantis et al. 2006). The eukaryotic plastidial sequences were taxonomical assigned using the Phytoref database of the plastidial 16S rRNA gene of photosynthetic eukaryotes (Decelle et al. 2015).

Plankton community size-fractionation experiments

Three plankton community fractionation experiments were performed; *Experiment 1* was initiated while the central fjord was still ice-covered (on 11th July), *Experiment 2* was initiated 4 d after the fjord became ice-free (19th July), and *Experiment 3* was initiated during autumn (16th September). We chose to collect water for the experiments from Sta. 3, as this was most accessible from Daneborg field station during ice-cover and at the same time with its central location it is representable for the fjord system as a whole. For each experiment, water (70–100 L) was collected at the Chl *a* maximum at Sta. 3 and directly gently syphoned into dark carboys. Prior to the setup, bottles and carboys were acid-washed and then rinsed in Milli-Q water. The treatments (hereafter: < 0.8, < 3, < 10, and < 90) were prepared by screening the water through either a 0.8 μm polycarbonate filter or a 3 μm, 10 μm, or 90 μm mesh filter by gentle reverse filtration in order to successively exclude protists of increasing sizes. Water for each treatment was gently transferred into triplicate 5-liter transparent foldable politainers (RPC Promens®) by staggered filling using silicone tubing. To mirror the seasonal change in mesozooplankton biomass in the fjord (Middelbo et al. 2018), Exp. 2 and 3 included additional treatments where mesozooplankton were added to < 90 μm filtered water. During Exp. 1, there were relatively few copepods present in the fjord (a biomass of < 0.5 mg C m^{-3}), therefore a treatment with copepod addition was not included. After the ice broke up copepod abundance increased up to 5 mg C m^{-3} (Middelbo et al. 2018) and a "copepod treatment" was included both in Exp. 2 and 3. As pelagic pteropods (snails) became abundant in autumn (up to 2 mg C m^{-3}), an additional treatment was included only in Exp. 3. In both Exp. 2 and 3, copepods (*Calanus hyperboreus* CVI) were added to a final abundance of 1 copepod L^{-1}. In Exp. 3, pteropods (*L. helicina*) were added to a final abundance of two individuals per 5-liter carboy. Hereafter, the treatments are referred to as "Copepod" and "Pteropod" ("Co" and "Pt" in Fig. 5). All individuals were alive after the 8–9 d of incubation.

The experimental carboys were incubated on a pier by the fjord in a 1000-liter PVC tank submerged in a flow-through water bath pumping water from the shore (1–3 m depth depending on the tide) to keep the temperature close to in situ surface temperature. The bottles were wrapped in dark nylon

mesh, reducing the irradiance to ~ 30% of surface PAR, similar to the light conditions at the depth at which they were collected. The bottles were rotated twice per day by hand. Every day, 50 mL sample (1% of total volume) was removed for the quantification of bacteria, small phytoplankton, and HNF. Every second day, 200 mL was additionally removed to measure bacterial production, FDOM, DOC, and inorganic nutrients. Further Chl *a* (> 0.7 μm [total], 2–10 μm and > 10 μm) and samples for enumeration of microsized protists were collected initially (T0), after 3 d and at the end of each experiment. Samples for 16S rRNA gene sequencing were collected from the < 90 treatment initially from Exp. 1 and Exp. 3 and from all treatments at the end of each experiment by filtering the remaining water onto 0.22 μm Sterivex filter (ca. 4 L) to enable comparison between the starting community and the effect of treatments by the end. The initial community from the < 90 treatment in Exp. 2 was lost and we, therefore, can only compare to the unfiltered in situ sample collected along with the experimental water. Exp. 1 was terminated after 5 d and Exp. 2 after 7.8 d and Exp. 3 after 9 d.

Net-growth rates (μ, d^{-1}) were calculated as the change in cell abundance (N) from the abundance at t_0 (N_0) to the abundance at sample time t_1 (N_1) as:

$$\mu = (\ln N_1 - \ln N_0)/(t_1 - t_0) \tag{1}$$

When protist grazing was reduced in the smaller size-fractions (i.e., < 0.8 and < 3), prey growth rate was higher ($\mu_{\text{no grazer}}$) than in the larger size-fractions, i.e., < 10 and < 90 where grazers are present ($\mu_{\text{with grazer}}$). Protist grazing (g, d^{-1}) could then be estimated by subtracting the two growth rates as:

$$g = \mu_{\text{no grazer}} - \mu_{\text{with grazer}} \tag{2}$$

It should be noted that the < 0.8 μm-filtration in Exp. 2 did not successfully exclude all picophytoplankton, small HNF and nanophytoplankton which all multiplied in the < 0.8-treatment (Supporting Information Fig. S1). The treatment was however still included in the further analysis as the HNF : Bac ratio was significantly reduced.

In the experiments, the change in FDOM intensity is calculated as:

$$\Delta \text{FDOM} = \frac{\text{FDOM}_X}{\text{FDOM}_0} - 1 \tag{3}$$

where FDOM$_0$ and FDOM$_X$ are the fluorescence intensities of each component averaged for all treatments at day 0 and the intensity averaged within each treatment at day X, respectively.

Statistical analysis

Redundancy analysis was done using primer-e version 6 (Plymouth, UK) and Canoco 5 (Ter Braak and Šmilauer 2012). multivariate analysis of variance (MANOVA and of covariance between depended variables, using a general linear model) was used to examine covariance between the five fluorescence components both in situ and in the experiments using the program R and the package "car" (Fox and Weisberg 2011).

Results

Hydrography, nutrients, and plankton

In the summer (July–August), terrestrial runoff created a clear halocline at 5–6 m with a layer of low salinity (< 20) water in the surface and more saline bottom water (> 30) (Fig. 2). In autumn (September–October), the runoff had ceased, and periodic storms followed, mixing the surface layer depth so that the mixed layer depth (MLD) extended to around 40 m and the near-surface water was colder (2°C). In general, the inner part of the fjord system was more stratified than the coastal shelf waters, but the wind mixing in October was enough to deepen the MLD in the entire fjord (Fig. 2). Phytoplankton Chl *a* fluorescence was most intense at 26–35 m depth at the outer fjord stations (3 and 4) in the summer period (up to 3.1 μg Chl *a* L^{-1}). At the innermost stations, the Chl *a* maximum was shallower (20 m) and concentrations were highest in late autumn (up to 1.6 μg Chl *a* L^{-1}) (Fig. 2, Supporting Information Fig. S2).

With respect to Redfield, oxidized nitrogen (NO$_x$) (0.26 $\pm$ 0.25 μM) was limiting relative to phosphate (P) (0.41 $\pm$ 0.19 μM) during both seasons in the upper mixed layer. Ammonium was only measured at Sta. 3 in the fjord and was at low concentrations ranging between 0.05 μM and 0.4 μM (avg. 0.27 $\pm$ 0.17 μM). In the rivers, phosphate was comparably low as in the fjord (0.3 $\pm$ 0.2 μM) but NO$_x$ was several fold higher (1.1 $\pm$ 0.5 μM). Silicate was elevated in the river water (avg. 17 $\pm$ 12 μM, max 46 μM) with increasing concentrations during the runoff period compared to the fjord surface values (2 $\pm$ 1.8 μM). The inner part of the fjord became ice-free prior to the central part. During the first sampling July Sta. 3 was still ice-covered, and there was a reduction in nutrients just below the ice (NO$_x$ = 0.01, P = 0.33, Si =1 μM) compared to deeper waters at 100 m (NO$_x$ = 3.2, P = 0.7, Si = 6.4 μM) indicating that a phytoplankton spring bloom had already started in the inner fjord.

The phytoplankton community differed between the inner fjord (Sta. 1 and 2) and the outer fjord (Sta. 3 and 4). In the outer part of the fjord, diatoms, mainly *Chaetoceros* sp., and autotrophic dinoflagellates dominated, while picophytoplankton dominated the inner fjord (Middelbo et al. 2018). Large and small heterotrophic HNFs also had different distribution patterns with large HNF being most abundant in the inner part of the fjord in autumn (max. 170 cell mL^{-1}, 63 $\pm$ 36 cell mL^{-1}), while small HNF generally were more abundant in summer, but without strong spatial variations (250 $\pm$ 155 cell mL^{-1}) (Supporting Information Fig. S2). Abundances of both HNF size groups were significantly reduced in the freshwater-influenced surface water compared to the more saline waters below (Supporting Information Fig. S2). Ciliate abundances

were also lower (3.4 ± 2.3 cells mL^{-1}) in 1 m samples than in deeper samples (data not shown). This resulted in a general low predator to prey ratio in the surface water during summer stratification (Fig. 6).

DOM distribution in the fjord and rivers

The average concentration of DOC was 100 ± 22 μM in the fjord (Supporting Information Fig. S2) and the rivers had significantly lower DOC concentrations (< 40 μM). Thus, the rivers diluted the upper 5 m of the fjord in terms of DOC. The three visible wavelength FDOM components displayed a similar vertical distribution with maximum intensities at 30–40 m and decreasing above 20 m, illustrated by C_{417} in Fig. 6. From summer to autumn, the intensity decreased in the upper 40 m. Visible FDOM signals were also generally lower at the outermost station at the shelf. The two UV FDOM signals exhibited a higher degree of variation and no distinct vertical patterns, as illustrated by C_{340} in Fig. 6, and the highest intensities of UV FDOM were measured in the central fjord (Sta. 2 and 3) (Fig. 6). When FDOM intensities were averaged within the different water types (Fig. 4), an ANOVA analysis of each component revealed that the visible fluorescent components were highly significantly different between water types (C_{417}: $p = 6.8 \times 10^{-6}$, C_{498}: $p = 2.7 \times 10^{-9}$, C_{405}: $p = 2.2 \times 10^{-6}$), whereas the UV fluorescent components were only marginally different (C_{340}: $p = 0.02$, C_{310}: $p = 0.04$). The seasonal change within water types revealed a significant decrease in C_{417} and C_{498} and UV fluorescent C_{340} from summer to autumn, as well as an increase in the fjord (Fig. 4). The fluorescence signal of the rivers had higher variation than in the fjord. The glacial rivers (R1 and R2) had the lowest intensity of visible fluorescence of all samples ($C_{498} = 0.04$–0.05 R.U.), and R3 during summer had the highest ($C_{498} = 0.13$ R.U.).

Links between bacteria and FDOM

In summer, bacterial abundances were lower in the fjord (ca. 4×10^5 cell mL^{-1}) than at the shelf (Sta. 4) (7×10^5 cell mL^{-1}) and peaked at 10 m just below the halocline at all stations (Fig. 6). In the central fjord, abundances increased significantly during the transition to autumn in the upper 40 m, whereas at the shelf station they did not change (Fig. 6 and Supporting Information Fig. S2). Similarly, BP was stable over the study period at the shelf, whereas in the fjord BP rates were higher (up to 2 μg C L^{-1} d^{-1}) in the summer than in autumn (< 0.2 μg C L^{-1} d^{-1}) (Fig. 6). As a result, the specific BP (production per cell) was on average more than twice as high in the fjord (averaged to 5.4×10^{-10} μg C d^{-1} cell^{-1}) than on the shelf (1.8×10^{-10} μg C d^{-1} cell^{-1}) (Supporting Information Fig. S2).

BP rates and several other environmental parameters were tested for correlations with the FDOM using Pearson's correlations (Table 1), in order to identify links between environmental factors and FDOM fluorescence. UV components C_{340} and C_{310} were positively correlated to Chl a and BP, but C_{417}, C_{498}, and C_{405} were strongest correlated to HNF : Bac and salinity and inversely correlated to bacterial abundance (Table 1).

To test the cumulative effect of all environmental parameters on the entire set of FDOM components and to identify the most influential variable, a redundancy analysis was performed separately for the two seasons with FDOM components as the dependent variables and environmental parameters as the explanatory variables (Fig. 7). In summer, the environmental parameters explained 53% of the total FDOM variation, with "HNF : Bac" (18%, $p = 0.002$) and "Chl a" (11%, $p = 0.008$) explaining most. In autumn, 42% of the FDOM variation could be explained, with "Salinity" (14%, $p = 0.008$) and the water type "Shelf water" (9%, $p = 0.004$) explaining most (Supporting Information Table S1). When a redundancy analysis was done for the entire data set the environmental variables were related similarly to FDOM, but with poorer explanatory power (Supporting Information Table S1).

Since bacteria can both produce and consume FDOM, we were further interested in whether FDOM components correlate with the abundance of the bacterial OTUs (Table 2). Several OTUs from different classes correlated both positively (e.g., *Balneatrix* and SAR92 clade) and negatively (e.g., *Litoricola* and SAR86 clade, SAR116 clade) to visible wavelength FDOM components. Only a few OTUs (e.g., *Colwellia* and SAR92 clade) correlated with the two UV FDOM components. The relative contribution (%) of OTUs that correlated positively to visible wavelength FDOM was especially high during summer, such as *Balneatrix* (10%) and SAR92 clade (11%). Interestingly, the genera that correlated strongly with visible FDOM signals did not correlate with salinity. The only genera that did correlate negatively with salinity (i.e., *Variovorax* and cyanobacteria) were freshwater taxa. In autumn, however, only a few OTUs correlated positively to visible wavelength FDOM and negative correlations were more common (Table 2).

In order to test whether the FDOM components might explain the changes in the composition of the bacterial community we applied another redundancy analysis. Here, the OTUs were the dependent variables and the FDOM components are the explanatory variables (Supporting Information Fig. S4). However, this analysis showed the FDOM components do not explain well the changes in the bacterial community composition. The only significant relationship on community level was found for UV FDOM component C_{340} in July ($p = 0.024$), where it explained 24.5% of the bacterial community composition.

Phytoplankton diversity in the experiments

The abundance of different size-classes of phytoplankton was successfully altered as part of the plankton community size fractionation manipulation (Fig. 5, Supporting Information Figs. S1, S3). In the first two experiments, *Chaetoceros* sp. dominated all size fractions larger than 10 μm, with
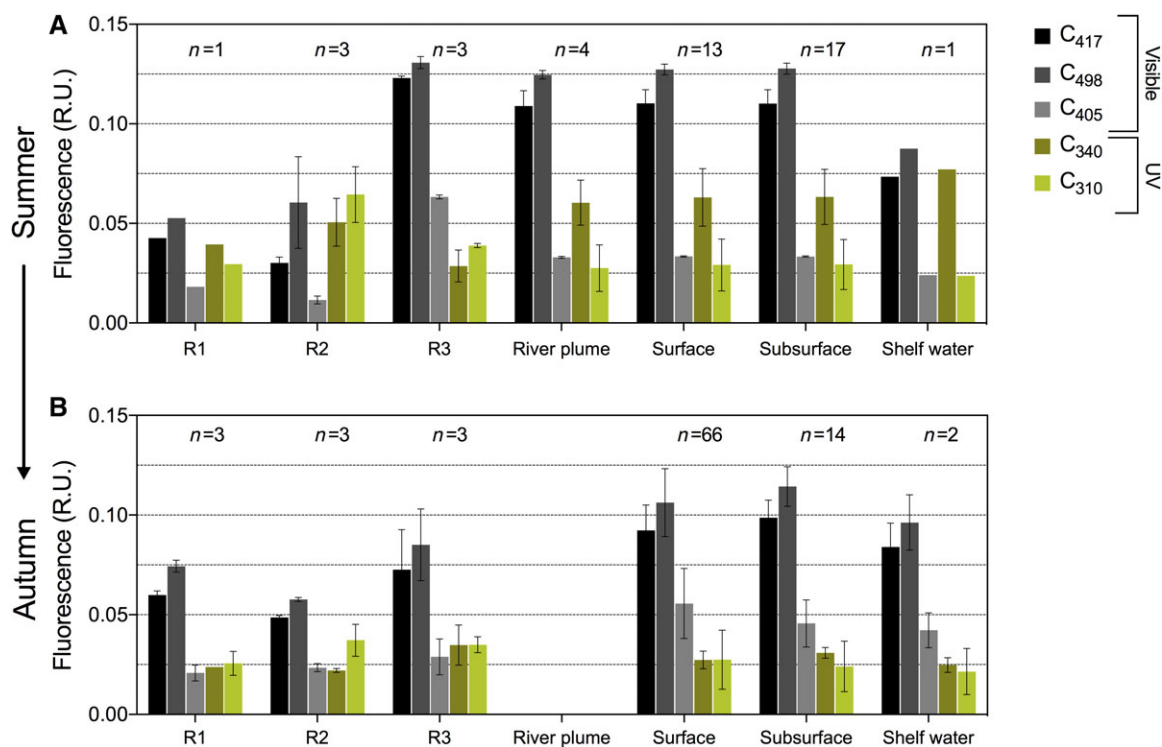
Fig. 4. The contribution of the three visible wavelength (gray) and two UV wavelength (green) FDOM components in the three rivers and in the fjord water types during (**A**) summer (July) and (**B**) autumn (September–October), values are shown as average ± SE, number of samples (*n*) given above the bars.

occasionally high contributions of silicoflagellates and chryso-phytes (Fig. 5A). The large Chl *a* fraction (> 10 μm) increased significantly in the treatments < 90 μm and the treatments with copepod addition, whereas in the treatments < 3 μm and < 10 μm the pico- and nanophytoplankton biomass increased (Fig. 5B). The third experiment (initiated in September) was dominated by pico- and nanosized phyto-plankton groups including silicoflagellates, cryptophytes, pra-sinophytes, and also the contribution of autotrophic dinoflagellates increased in autumn (Fig. 5A). Microsized dia-toms contributed little to the biomass in Exp. 3 (maximum 10–20% in the treatments with mesozooplankton) despite rel-atively high SiO_4 concentrations (4 μM), compared to Exp. 1 and 2, where silicate was reduced to < 1.7 μM and thus in lim-iting concentrations according to Egge and Aksnes (1992). NH_4^+ increased only in the mesozooplankton amended treat-ments in Exp. 3; with a gradual increase from 0.2 μM to 1.7 ± 0.4 μM in the pteropod treatment and an increased from 0.2 μM to 0.5 ± 0.03 μM in the copepod treatment, fol-lowing a decrease after 5 d (Fig. 5B, Supporting Information Fig. S1). Chl *a* in the 2–10 μm fraction doubled in the treat-ment with mesozooplankton, while it significantly decreased in the treatments with protists as top predators. Heterotrophic dinoflagellates dominated over ciliates numerically, especially in Exp. 1 and 2, during which the diatoms dominated the phytoplankton biomass (Supporting Information Fig. S3).

Bacterial diversity, growth, and grazing in experiments

The order Alteromonadales (genera *Glaciecola*, *Colwellia*, *Pseudoalteromnas*, and the SAR92 clade) dominated the bacte-rial community in Exp. 1 (46% ± 2%) and Exp. 2 (48% ± 10%)). Exp. 3 was dominated by the order Oceanos-pirillales (29% ± 10%) and was in general more diverse with a higher number of unassigned OTUs than in the two other experiments (27% ± 6%) (Fig. 5C). The genus *Glacieocola* var-ied most throughout the season and contributed as much as 33–36% in the first experiments whereas Exp. 3 only con-tained up to 4% *Glaciecola*. In treatments where mesozoo-plankton were added the Alteromonadales genera became more abundant with *Colwellia* (22–23%) and *Pseudoalteromo-nas* (10–21%) being most prominent. Oceanospirillales (*Balneatrix*, *Oleispira*, and the SAR86 clade) dominated when protists were the only grazers.

The treatments < 3 μm, 10 μm, and 90 μm were grouped into one treatment: "plus protists" in Figs. 8,9, as we found no significant differences between the three in regards to FDOM development (Supporting Information Fig. S6) nor in the abun-dance of bacteria and BP (Supporting Information Fig. S1). Like-wise, the treatments with addition of copepods and pelagic pteropods were grouped as "plus mesozooplankton." The 0.8 μm-filtration resulted in a reduction of the bacterial abun-dance at day 0 (Fig. 8A–C). In summer, the abundance was reduced by around 18% and in Exp. 3 as much as 40–45%,
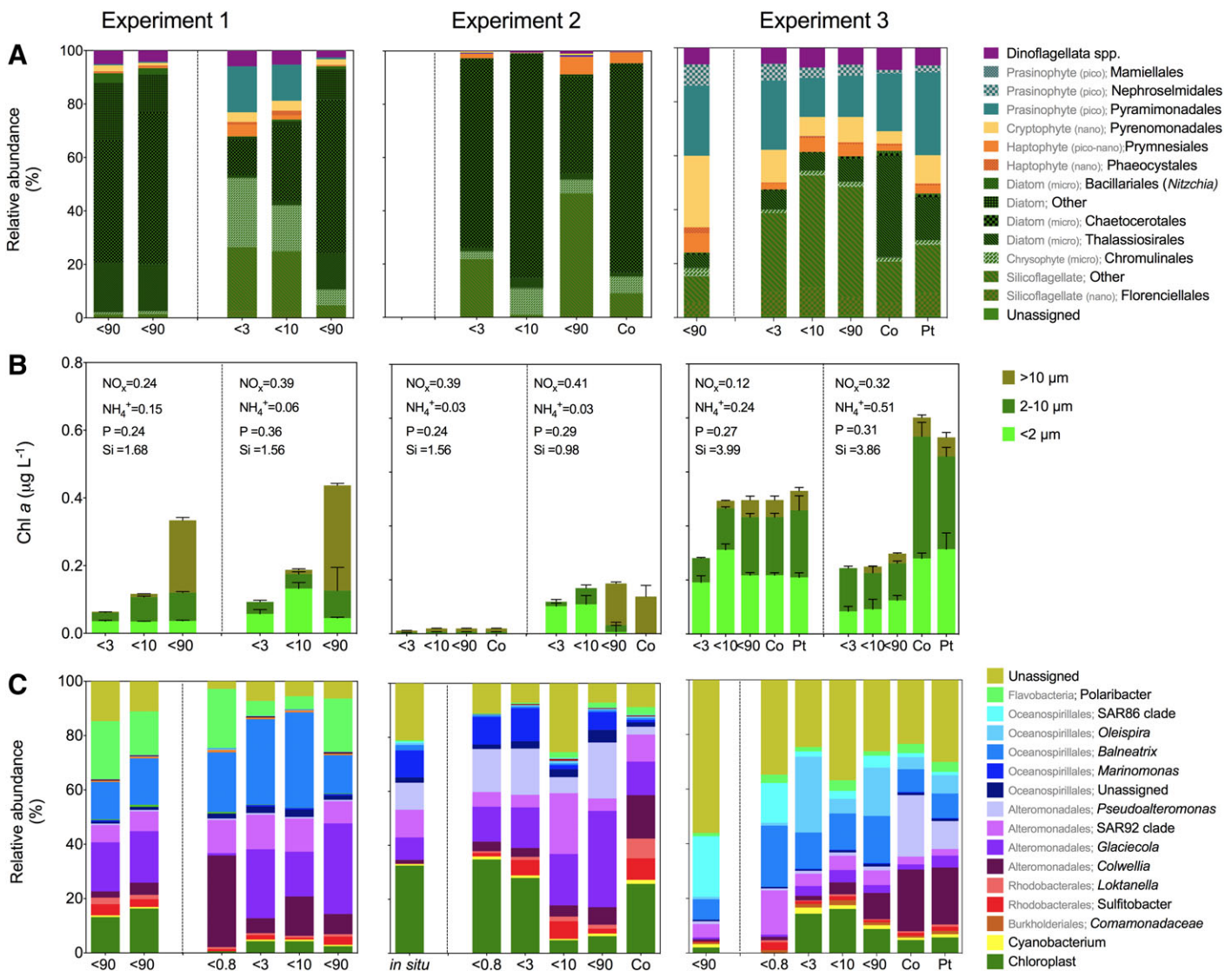
Fig. 5. The abundance of different size-classes of protists in the three incubation experiments. Initial and final values are given on the left and right-hand side of the dashed line, respectively. Duration was 5 d, 7.8 d, and 9 d of Exp. 1, 2 and 3, respectively. (**A**) Relative abundance of the most abundant phytoplankton species (phylum [size class]; order) based on plastidial 16S rRNA gene sequence data, showing the taxonomic diversity. (**B**) Chl *a* fractions (< 2 μm, 2–10 μm, and > 10 μm) and initial and end nutrient concentration for all treatments (average ± SD). (**C**) Bacterial community composition of the 15 most abundant taxa at genus level (order; genus) in the three incubation experiments. N.B. there are no initial molecular data from Exp. 2 only from unfiltered in situ water.

indicating that bacteria were larger in autumn than in summer. The abundance of bacteria in the 3 μm, 10 μm, and 90 μm filtered water at the beginning of the experiments were also around four times higher in autumn (9×10^5 mL^{-1}) than in the summer experiments (1.9×10^5 mL^{-1} and 2.6×10^5 mL^{-1}). Bacterial production increased from 0.5 μg C^{-1} L^{-1} d^{-1} to 6.3 μg C^{-1} L^{-1} d^{-1} within the first 3 d of incubation in the summer experiments (Fig. 8D,E), while in autumn (Exp. 3) BP remained less than 1.2 μg C^{-1} L^{-1} d^{-1} during the entire experiment. The predator-prey ratio (HNF : Bac $\times 10^3$ in Fig. 8, see also HNF numbers in Supporting Information Fig. S1) was reduced to near zero in the fraction with only bacteria, except in Exp. 2.

The ratio remained between 1 and 5 (i.e., 1000–5000 bacteria per HNF) in treatments with protists and mesozooplankton, except for the end of Exp. 2 where it increased to 14 in the treatments with protists (Fig. 8G–I). On the whole, this indicates that the experimental size fractionation successfully released grazing pressure so that we could differentiate between FDOM changes due to bacterial degradation and those due to grazing.

Grazing rates of bacteria (calculated by Eq. 2), picophytoplankton and HNF were highest in summer and very similar between Exp. 1 and 2 (Supporting Information Table S2). The net-grazing on bacteria correlated strongly to HNF : Bac in all experiments (r^2 = 0.82, 0.59, and 0.77; $p < 0.0001$, for Exp. 1,

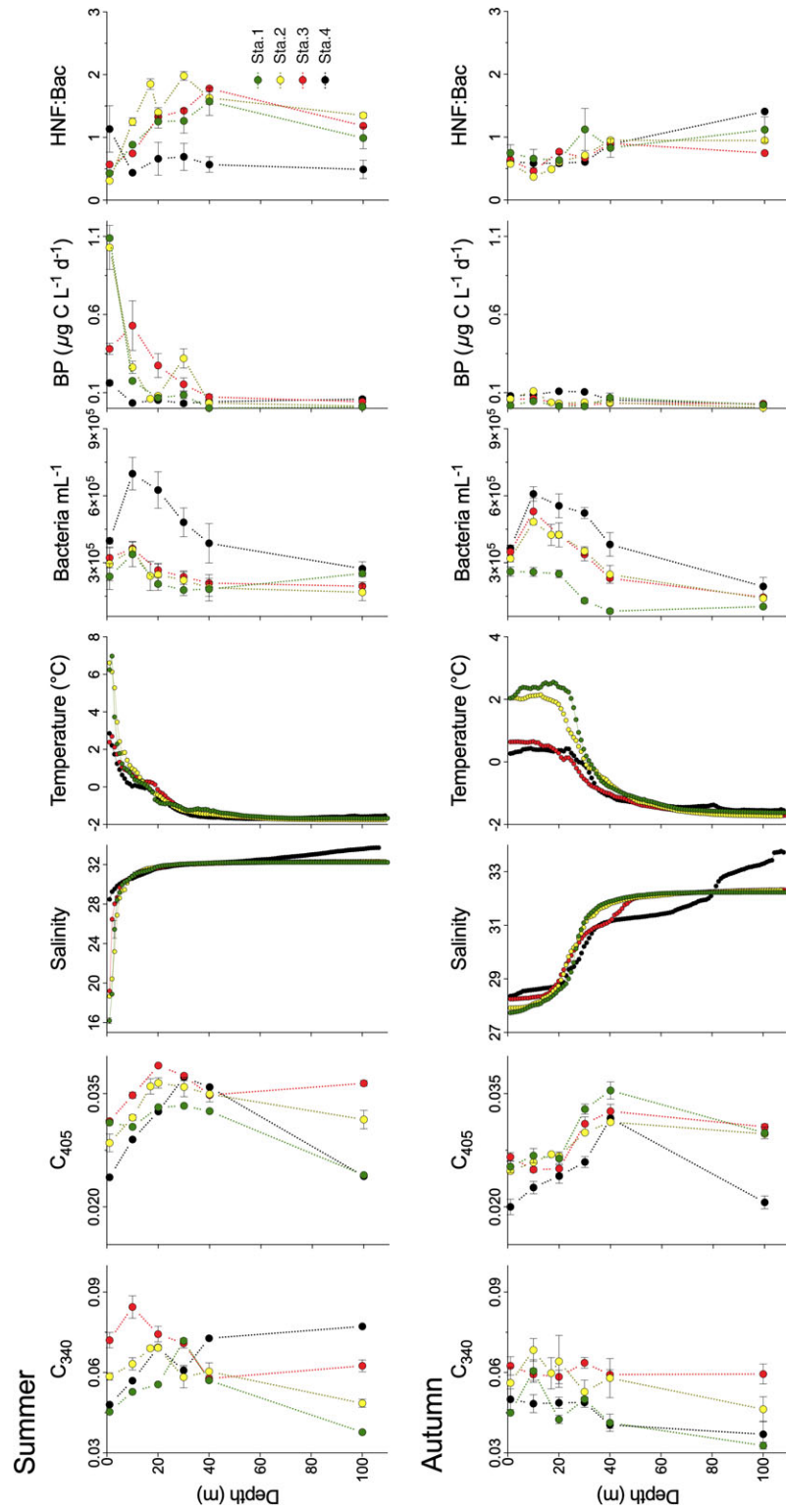**Fig. 6.** Profiles of the UV wavelength C_{340} and the visible wavelength C_{405} FDOM components, salinity and temperature (°C), bacterial abundance (cells mL^{-1}), bacterial production (μg L^{-1} d^{-1}), and the grazer to prey ratio (HNF : Bac) in the upper 100 m of the fjord stations; Sta. 1 (green), Sta. 2 (yellow), Sta. 3 (red), and Sta. 4 (black). Values are shown as average $\pm$ SE of 3–4 profiles sampled within the summer (upper panel) and autumn period (bottom panel). Note different x-axis for salinity and temperature in the two periods.

Table 1. Pearson correlation coefficient, *r*, for the linear association between the FDOM components and environmental and biological variables are given for the two seasons from in situ observations from the four fjord stations. Red indicates negative and green positive associations. Significant relationships are marked by *.

| | Summer | | | | | Autumn | | | | |
| | Visible wavelength | | | UV wavelength | | Visible wavelength | | | UV wavelength | |
	C_{417}	C_{498}	C_{405}	C_{340}	C_{310}	C_{417}	C_{498}	C_{405}	C_{340}	C_{310}
HNF:Bac	0.54 **	0.47*	0.49**	−0.05	0.15	−0.03	0.04	0.14	-0.38*	−0.20
Chl *a*	0.44 *	0.45*	0.46*	0.22*	0.19	0.15	0.14	0.03	0.19	0.10
Salinity	0.41*	0.40*	0.31*	0.16	0.07	0.37*	0.43**	0.51**	−0.14	−0.10
BA	−0.16	−0.22*	−0.10	0.07	−0.05	−0.36*	−0.39*	−0.52**	0.14	0.12
BP	−0.20*	−0.18	−0.11	0.19	0.12	0.24*	0.26*	0.14	0.27*	0.24*
BDOC	−0.08	−0.11	−0.28*	0.33*	−0.02	−0.09	−0.10	−0.08	−0.08	0.15

2 and 3, respectively; Supporting Information Fig. S5). We, therefore, consider HNF : Bac to be an appropriate indicator of bacterial grazing in our system.

Consumption and production of FDOM in the experiments

As a result of the changing seasonal conditions in the fjord, the three size-fractionation experiments were initiated with fjord water differing significantly in initial FDOM composition (two-way ANOVA, $p < 0.0001$) (Fig. 9, left panel). We observed a strong significant difference in development of FDOM between the experiments (MANOVA: $F_{2,122} = 0.55$, $p < 0.00001$, partial eta squared = 0.28).

During the incubation, the relative change in intensity (calculated by Eq. 3) differed between the visible and UV wavelength FDOM components (Fig. 9). The UV FDOM increased in all experiments, mainly in Exp. 2 during which the initial UV FDOM intensity was close to zero. C_{310} was often produced at high rates in the treatment with only bacteria (Fig. 9). Mesozooplankton addition to the incubations resulted in elevated UV FDOM intensities after 3.7 d in Exp. 2 and by 2.8 d in Exp. 3, with the addition of the pteropod *L. helicina* having a slightly higher effect than copepods (Supporting Information Fig. S6).

The visible wavelength FDOM components developed differently in the two seasons. In summer (Exp. 1 and 2), we observed a gradual decrease (i.e., consumption or transformation) of all components, while in autumn (Exp. 3), they were produced. In general, C_{417} was consumed at lower rates and
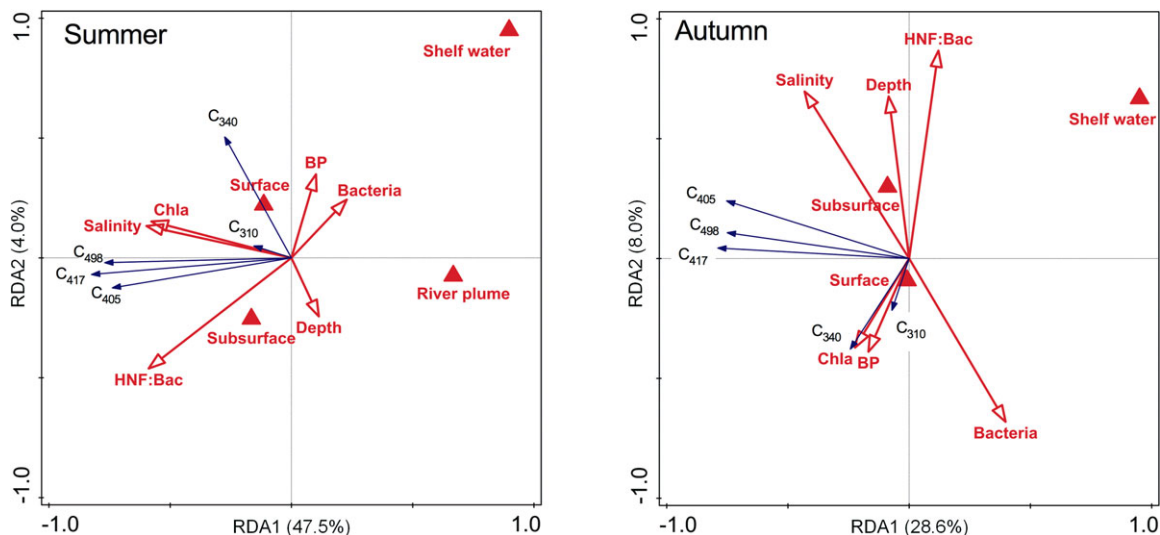

Fig. 7. Redundancy analysis biplot summarizing the variation of the five FDOM components in summer and autumn from in situ samples (dark blue arrows) in response to selected environmental and biological variables (red arrows) and to the water type as a categorical value (red triangles).

Table 2. Pearson correlation coefficient, *r*, for the positive (green) and negative (red) linear association between selected OTUs of bacteria (based on plastidial 16S rRNA sequence data), and the five FDOM components and salinity in the entire fjord data set (not including the rivers). Significant relationships are marked by *. The OTU number, the assigned order, and genera/clade are given in the three first columns. The 4th column indicates the relative abundance of each OTU as the sum of reads out of the total (green = high abundance, red = low abundance) separated into summer (July) and autumn (September).

| Order | OTU# | Genus/ taxa | Percentage of community | | Visible FDOM | | | UV FDOM | | |
			Summer	Autumn	C_{417}	C_{498}	C_{405}	C_{340}	C_{310}	Salinity
Alteromonadales	37,117	Glaciecola	0.3	0	0.42*	0.44*	0.25	0.34	0.34	−0.02
Alteromonadales	25,156	SAR92 clade	0.2	0	0.57**	0.55**	0.71****	0.43*	0.28	−0.01
Alteromonadales	31,010	SAR92 clade	10.9	2.6	0.46*	0.45*	0.62***	0.3	0.17	−0.33
Alteromonadales	154,480	SAR92 clade	0.3	0.1	0.51**	0.55**	0.56**	0.48*	0.34	0.08
Alteromonadales	1564	SAR92 clade	1	0.1	0.6***	0.6***	0.5**	0.40*	0.40*	−0.04
Oceanospirillales	50,365	uncultured	0.2	0.2	0.53**	0.59***	0.31	0.18	0.18	0.41*
Oceanospirillales	133,547	Balneatrix	9.5	3.9	0.39*	0.36	0.29	0.25	0.25	0.08
Oceanospirillales	71,739	Balneatrix	0.3	0	0.57**	0.55**	0.75****	0.47*	0.36	−0.04
Oceanospirillales	36,864	Balneatrix	0.2	0.1	0.49**	0.49**	0.43*	0.22	0.19	0.19
Oceanospirillales	96,009	Balneatrix	1.4	0.2	0.5**	0.47*	0.38*	0.32	0.32	0.08
Methylophilales	121,499	Methylotenera	0.4	0.1	0	0	0.22	−0.04	0.06	−0.62***
Alteromonadales	107,394	Colwellia	0.6	0	0.43*	0.43*	0.51**	0.52**	0.26	0.18
Cyanobacterium	118,758	uncultured	0.6	0	0.04	0.01	0.19	−0.04	−0.11	−0.64***
Alteromonadales	162,434	Glaciecola	0.9	0.3	0.04	−0.02	0.06	−0.24	−0.39*	−0.4
Burkholderiales	157,176	Variovorax	0.4	0	−0.08	−0.07	0.17	−0.15	0.03	−0.76****
Flavobacteriales	70,100	NS5	0.2	1.6	−0.48**	−0.45*	−0.31	−0.29	−0.29	−0.5**
Oceanospirillales	16,552	Litoricola	0.2	1.3	−0.54**	−0.51**	−0.68****	−0.41*	−0.35	0.22
KI89A	53,876	uncultured	0.2	1.6	−0.58**	−0.56**	−0.72****	−0.37	−0.32	0.21
Alteromonadales	71,481	Porticoccus	0.2	1.5	−0.53**	−0.49**	−0.66***	−0.25	−0.19	0.2
Oceanospirillales	41,665	uncultured	0.5	0.6	−0.57**	−0.51**	−0.42*	−0.46*	−0.14	−0.59***
Cyanobacterium	110,706	uncultured	2.8	0.9	−0.31	−0.24	−0.08	−0.2	0.12	−0.67***
Rhodospirillales	145,914	AEGEAN169	0.5	2	−0.51**	−0.48**	−0.65***	−0.31	−0.26	0.12
Rickettsiales	45,394	SAR116 clade	1.2	3.5	−0.45*	−0.43*	−0.29	−0.29	−0.29	0.09
Rhodobacterales	20,147	Rhodobacter	0.9	1.8	−0.5**	−0.48*	−0.53**	−0.28	−0.22	0.02
Burkholderiales	50,758	Variovorax	8.4	0.2	−0.09	−0.07	0.15	−0.17	0.01	−0.76
Oceanospirillales	62,656	SAR86 clade	0.6	2.3	−0.42*	−0.40*	−0.22	−0.16	−0.16	0.26
Oceanospirillales	37,238	SAR86 clade	0.7	5	−0.55**	−0.52**	−0.69****	−0.31	−0.27	0.24

produced at higher rates than C_{498} (Fig. 9). The highest consumption rates were measured in Exp. 1. In Exp. 2, visible wavelength FDOM decreased the most in the treatment with only bacteria, while the presence of mesozooplankton grazers even stimulated a small net-production of C_{417} and C_{405} during the first 3 d (Fig. 9E). In Exp. 3, there was no net-consumption of FDOM, but production rates were almost twice as high in grazer-treatments than in the "bacteria only" treatments after 7.5 d (Fig. 9F–K). We observed that the change in visible wavelength FDOM correlated negatively to

bacterial net-growth (Eq. 1) in the summer experiments (Exp. 1: $r^2 = 0.62$, $p < 0.0001$, Exp. 2: $r^2 = 0.32$, $p = 0.0008$), and a positively to grazing on bacteria in all experiments (Exp. 1: $r^2 = 0.45$, $p = 0.0034$, Exp. 2: $r^2 = 0.43$, $p = 0.0005$, Exp. 3: $r^2 = 0.19$, $p = 0.017$).

Overall, in Exp. 1, the presence of grazers affected the rate of change in FDOM intensity during the first 3 d, whereas all the different treatments essentially arrived at similar net-change of FDOM intensity after 5 d. In Exp. 2, the decrease in visible FDOM was lowest in treatments with grazers whereas
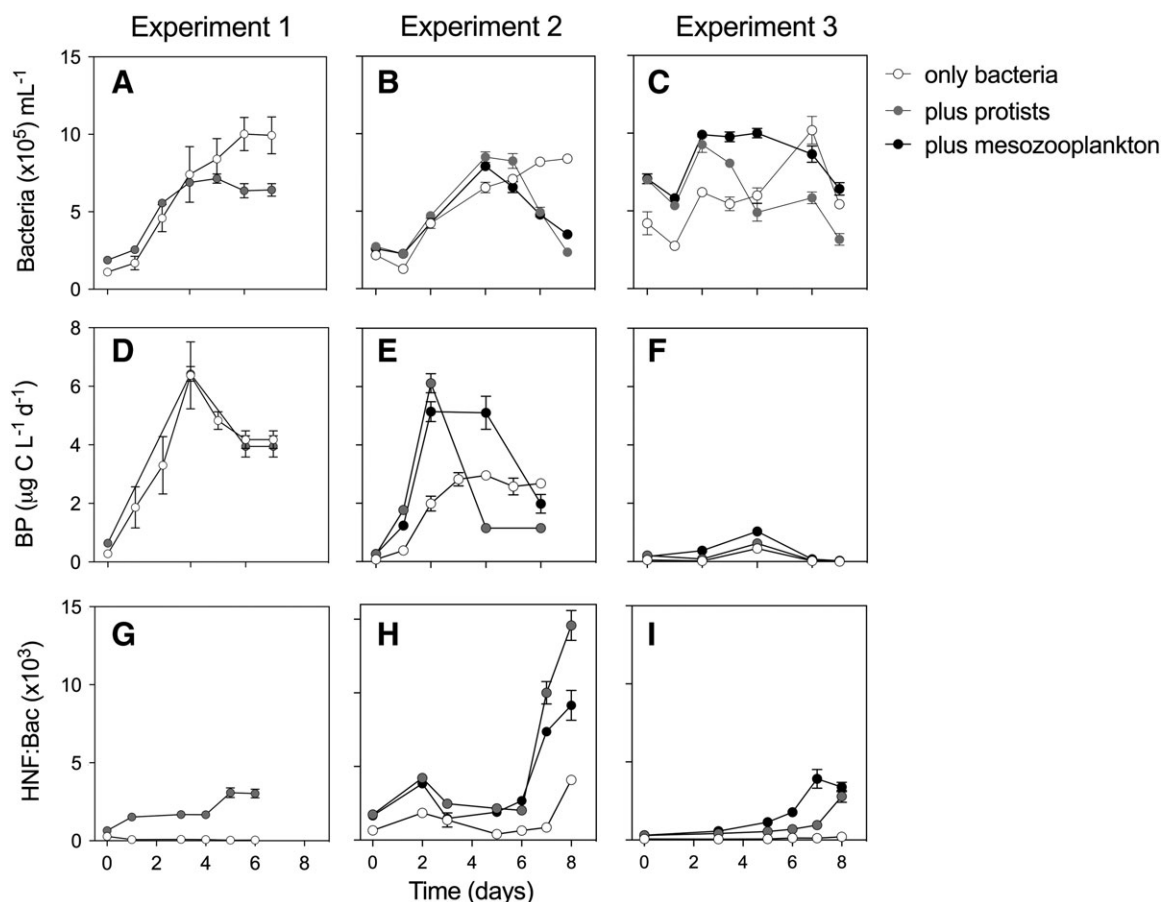
Fig. 8. (**A–C**) The change in bacterial abundance ($\times 10^5$) mL^{-1}, (**D–F**) bacterial production (μg C L^{-1} d^{-1}), and (**G–I**) predator to prey ratio HNF : Bac ($\times 10^3$) during the course of the three experiments.

the production of UV FDOM was clearly stimulated by their presence. In Exp. 3, where bacterial activity was low, visible FDOM was produced in all treatments and the positive effect of grazers on FDOM change remained significant after 7.5 d.

Discussion

FDOM properties have been used as water mass indicator, and especially the "humic-like" FDOM characterized with emission maxima at visible wavelengths is often considered to be refractory and therefore used as a conservative tracer (Catalá et al. 2015). Yet, the imprint that marine microbes have on FDOM remains poorly resolved. The data collected here provides an opportunity to examine the interplay between biological activity and hydrography on the distribution and composition of FDOM. In this light, the FDOM signal can be used as an indicator revealing the dynamics of DOM production, consumption, and transformation in the fjord system.

FDOM dilution by glacial meltwater

Surprising and in contrast to most fjord systems, visible wavelength FDOM correlated positively to salinity (Fig. 7)

indicating that the marine end-member is the important FDOM source rather than the local runoff. The reduced intensity of visible wavelength FDOM in the freshwater influenced surface layer could potentially also have been caused by photochemical degradation (Ward et al. 2014; Aarnos et al. 2018). However, as the ice in the Young Sound fjord system disappears after the summer solstice, the sun angle is also decreasing rapidly and as a result, the inner fjord system is shaded by surrounding mountains preventing direct exposure. Thus, the likely impact of photochemical degradation is probably limited in Young Sound. In addition, light penetration is inhibited by the silty runoff that increases turbidity in the fjord (Murray et al. 2015), mainly early in the ice-free period.

The FDOM signal from local terrestrial runoff is difficult to resolve, as FDOM intensity, DOC concentrations, and bioavailability can fluctuate (Kroon et al. 2017; Paulsen et al. 2017) in response to episodic input events which are easily be missed when sampling. However, the low fluorescence intensity of riverine FDOM measured 16 times from July to September strongly suggests that the rivers are not a major contributor of carbon or of FDOM in the system but rather dilute FDOM in the fjord. This is in strong contrast to the
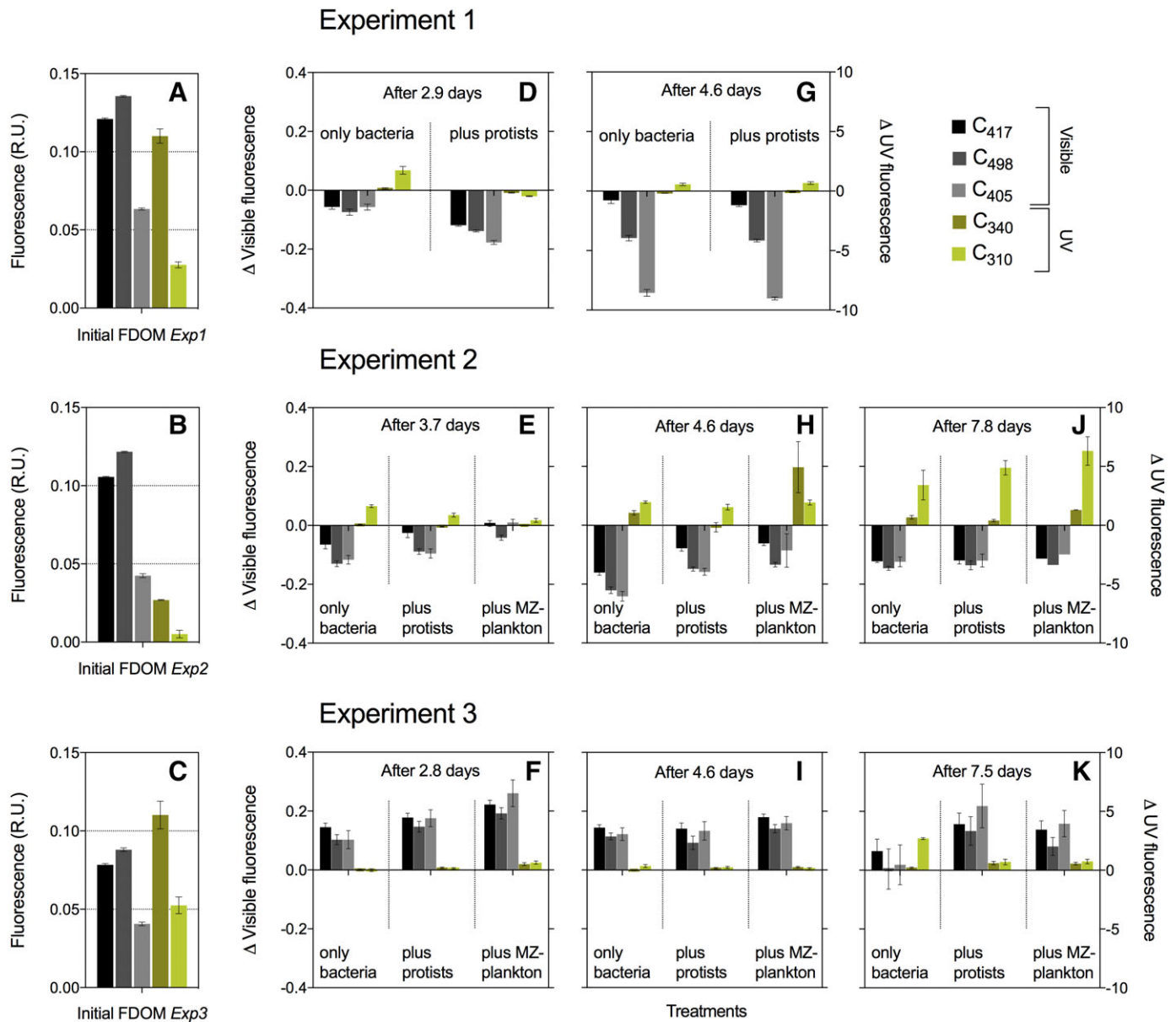
Fig. 9. (**A–C**) The initial intensity of the three visible wavelength (gray) and two UV wavelength (green) FDOM components in the three experiments. (**D–K**) The change in FDOM fluorescence in the different treatment "only bacteria," "plus protists," and "plus mesozooplankton" calculated by Eq. 3 for the approximately time intervals 0–3, day 0–5, and day 0–7.

majority of Arctic rivers, which are important sources of carbon and visible FDOM with as high as 1.8 nm^{-1} (Walker et al. 2013). In comparison, the highest intensity of visible fluorescence sampled in the Young Sound was 0.08 nm^{-1} in the glacial rivers and 0.13 nm^{-1} in R3.

The FDOM signals from the three rivers were directly related to their catchment, with the glacial rivers R1 and R2 supplying similar and low signal, while the tundra and lakes in the R3 catchment supply an elevated and more variable signal. Similar variations in FDOM intensity of large Arctic rivers have been explained by the difference in the vegetation characteristics of the catchment (Walker et al. 2013),

further the presence of proglacial lakes results in higher DOC concentrations (340–406 μM C) (Bhatia et al. 2010; Hauptmann et al. 2016). The low-carbon content in glacial meltwater in Young Sound is consistent previous observations from the western part of Greenland Ice Sheet with 7–32 μM C, 15–51 μM C, and 21–100 μM C found in subglacial, supraglacial discharge, and a glacial stream with connection to a proglacial lake, respectively (Bhatia et al. 2010; Lawson et al. 2014; Hauptmann et al. 2016). In terms of carbon concentration and FDOM, the runoff connected to Greenland glaciers thus rather dilutes, than contributes, to the fjord system.

Coastal water as a source of visible FDOM

The shelf water in the East Greenland region is characterized by three general layers (Sejr et al. 2017): (1) *Re-circulating Atlantic water* ($T > 0°C$) at depths greater than 200 m (not sampled in the current study), (2) *Polar water* that originates from the Polar halocline transported from the Arctic Ocean in the East Greenland Current ($T < 0°C$, $S \sim 31$–32), and (3) *Surface waters* ($S < 25$), which are modified locally by the inclusion of meltwater from sea ice and the Greenland Ice Sheet in summer. The overall distribution of visible FDOM was hydrographically driven by the high-signal intrusion of Polar water terrestrial DOM from the marine end-member and dilution by low-signal glacial runoff in the surface.

The fluorescence characteristics of visible FDOM C_{498} reported here is identical to "C1" described on the Greenland Shelf outside of Young Sound by Gonçalves-Araujo et al. (2016) (Tucker's congruence coefficient Em/Ex = 0.96/0.97), who also linked this signal to organic matter in Polar water. The intensity of C_{498} found on the Greenland Shelf (0–300 m) in September ranged from 0 nm^{-1} to 0.1 nm^{-1} and is thus not higher than our measurements within the subsurface water in Young Sound in September (range: 0.09–0.16 nm^{-1}, avg.: 0.12 ± 0.02 nm^{-1}, $n = 30$). This suggests that Polar water is not the only source of the high visible fluorescence signal associated with waters in the depth range of 20–40 m, but rather local biological productivity. It seems that autochthonously produced visible wavelength FDOM is indistinguishable from the allochthonous component of terrestrial FDOM in Polar waters found in the East Greenland Shelf. Thus, the visible wavelength components identified from EEMs cannot serve as a conservative tracer of DOM alone as suggested by Gonçalves-Araujo et al. (2016). Our results indicate that local microbial productivity contributes to altering the signal and thus although behaving conservatively during its passage across the Arctic, microbial productivity at coastal sites stimulates both the production and degradation of visible FDOM.

Biological production of visible wavelength FDOM

In the fjord, the intensity of the visible wavelength fluorescence signals correlated positively to Chl *a* and HNF : Bac in summer and positively to salinity in autumn (Fig. 7; Table 1). This seasonal change may best be explained by the change in biological activity; in summer, high-primary production, bacterial growth, and high-grazing rates results in an accumulation of visible wavelength FDOM in the subsurface fjord water. When biological processes were low in autumn, the hydrographical distribution of visible FDOM became more obvious as indicated by the strong positive relationship between salinity and visible FDOM in this period (Table 1). Our experimental results during autumn (Exp. 3), together with the previous work by Baña et al. (2014), suggest that that the presence of grazers increases the production of visible wavelength FDOM. We hypothesize that the reason for the increase in Exp. 3 is that the bacterial growth was so low that

the production of visible fluorescence due to bacterial grazing exceeded the bacterial consumption. Also, in Exp. 3, there were more and larger bacteria (and thus even higher bacterial biomass than suggested by just their numbers) than during the summer experiments (Fig. 8A–C).

A link between UV FDOM and mesozooplankton

The UV FDOM signals have been linked to phytoplankton abundance (e.g., Chl *a*) (Lønborg et al. 2014; Gonçalves-Araujo et al. 2016) as well as to water mass mixing (Catalá et al. 2016). In Young Sound, their variability was best explained by productivity related parameters such as Chl *a* and BP (Fig. 7; Table 1), although correlations with UV FDOM were weaker than those of visible FDOM (Table 1). The high production of UV FDOM associated with the presence of mesozooplankton in the experiments (Fig. 9) was in agreement with the in situ fluorescence intensities being highest in the central fjord (Sta. 2 and 3), where maximum copepod activity was recorded (Middelbo et al. 2018). When performing linear regression analysis between our UV FDOM intensity and copepod biomass, fecal pellet production and egg production published in Middelbo et al. (2018), we found a weak positive correlation between specific fecal pellet production and C_{310} ($r^2 = 0.26$, $p = 0.03$, $n = 19$), while there was a stronger correlation when comparing to the community fecal pellet production for both UV components (C_{340}: $r^2 = 0.35$, $p = 0.008$, C_{310}: $r^2 = 0.34$, $p = 0.009$). However, there was no correlation of UV FDOM to copepod biomass, nor between the visible fluorescent components and any copepod related parameters. Although the correlations with copepod activity were relatively weak, copepod activity relates better to the UV fluorescence than to any other environmental parameter, and we speculate that this is due to sloppy feeding, excretion and leakage from fecal pellets as found in other studies (Poulet et al. 1991; Møller et al. 2003; Urban-Rich et al. 2004; Møller 2007), and possibly, bacterial degradation of organic matter associated with grazing. Our experimental work further demonstrated that the pelagic pteropod *L. helicina* could have a similar, or even stronger effects, on FDOM transformations as well as NH_4^+ production.

Bacterial consumption of visible wavelength FDOM

Visible wavelength FDOM decreased markedly in the fjord from summer to autumn (Figs. 4, 6). The deepening of the mixed layer caused by autumn storms can partly account for the reduction in subsurface visible FDOM (Fig. 6). However, if the autumn mixing were the only explanation, a corresponding increase in visible FDOM at the surface (1 m) would be expected, which was not the case. The decrease in visible wavelength FDOM co-occurred with a net-increase in bacterial abundance. This is seen as a negative correlation between visible FDOM and bacterial abundance (Table 1) and indicates a net uptake or transformation of visible fluorescent components by bacteria. This is further supported by relatively

higher subsurface bacterial production in the fjord (Sta. 1–3) in summer when visible wavelength FDOM intensities were high, compared to autumn. Moreover, the incubation experiments demonstrated a decrease in visible FDOM when bacterial growth was high in summer (Exp. 1 and 2). The consumption of visible FDOM in these experiments is supported by a similar experiment from the Alaskan Arctic by Sipler et al. (2017), where they found consumption (7% within 4–6 d) of "humic-like" terrestrial-derived DOM.

As the change in FDOM in the "only bacteria treatment" was similar to the change in treatments with larger organisms, bacteria are likely the main decomposers of visible wavelength DOM. Certain bacterial taxa, especially within the class Gammaproteobacteria, are commonly known to degrade a wide range of different carbon sources, including high-molecular weight terrestrial DOM (Sosa et al. 2015; Sipler et al. 2017), and can occur at high concentrations in coastal environments. Predominantly taxa from this class, such as *Glaciecola* spp., *Balneatrix*, and the SAR92 clade dominated the summer experiments (Fig. 5) and were highly abundant in the fjord in July (Table 2), and thus further supports our finding that Young Sound residing bacterial community was able to degrade humic-like visible wavelength FDOM. Interestingly, however, we found that not all taxa belonging to Gammaproteobacteria showed a positive correlation with visible wavelength FDOM. Especially the order Oceanospirillales was more abundant in autumn and correlated negatively to visible wavelength FDOM as previously observed also in river DOM in Arctic Alaska by Sipler et al. (2017) who further reported there to be no influence of river DOM (positive or negative) on the bacterial community down to the phylogenetic level of "order." We saw the same noncoherent tendency with OTUs belonging to the same genus but having different correlation patterns, i.e., most *Glaciecola* OTUs correlated positively with visible wavelength FDOM, but few correlated negatively (Table 2). Such different functional behavior between clades and strains within the same genus calls for future work focusing on linking bacterial function rather than diversity to DOM turnover.

Our study stresses that bacterial community composition and functioning are central for the bioavailability of FDOM and contradict the view that visible wavelength FDOM, in general, is refractory to bacteria. Measurements of %BDOC reveal that the subsurface fjord water had the lowest bioavailability (5.3% ± 1.8%; Paulsen et al. 2017) and it is tempting to conclude that the low bioavailability is connected to the high contribution of visible FDOM in this water mass. However, we here find a rapid planktonic transformation of visible FDOM from subsurface fjord water during the summer period. Though the loss of FDOM is not a quantitative measure of carbon remineralization, it can be used as a sensitive indicator of DOM processing occurring at levels below the detection limits of DOC measurements. We therefore speculate that the BDOC method underestimates the in situ potential for degradation of visible FDOM. This method relies on long-term incubations

and as a result an altered bacterial community composition (Müller et al. 2018) and function, which as a consequence likely reduces the ability to degrade visible FDOM. In contrast, the method applied here has a bacterial community more representative of natural conditions in the fjord and reveals their potential to degrade visible FDOM. An underestimation of the in situ carbon degradation by the BDOC method implies that the significant amounts of BDOC in glacial runoff reported by Hood et al. (2009), Fellman et al. (2010), and Lawson et al. (2014), may, in fact, be negligible compared to the degradation potential of the various autochthonous carbon sources that are already present in the fjord.

Conclusions

The low visible FDOM signal of the glacial runoff indicated that the rivers contributed to a seasonal dilution of DOM and FDOM in the surface waters, whereas the more saline coastal water (transported from the Arctic Ocean) had a higher content of visible FDOM. In this light, the NE Greenland fjord systems are unique in the sense that the dominant source of terrestrial organic matter comes from the marine end-member. The high biological productivity period resulted in an elevated visible FDOM signal in the fjord subsurface. The degradation of visible FDOM appears to be linked to specific bacterial taxa (*Glaciecola* spp., *Balneatrix*, and the SAR92 clade) and there is a lack of coherency down to the order level suggesting that clades and strains within the same genus may have different functional behavior. Although bacteria are the major decomposers of FDOM, the dynamics of FDOM depends on grazing at protozoan and metazooplankton levels.

References

Aarnos, H., Y. Gélinas, V. Kasurinen, Y. Gu, V.-M. Puupponen, and A. V. Vähätalo. 2018. Photochemical mineralization of terrigenous DOC to dissolved inorganic carbon in ocean. Global Biogeochem. Cycles **32**: 250–266. doi:10.1002/2017GB005698

Amon, R. M. W., G. Budéus, and B. Meon. 2003. Dissolved organic carbon distribution and origin in the Nordic Seas : Exchanges with the Arctic Ocean and the North Atlantic. J. Geophys. Res. **108**: 1–17. doi:10.1029/2002JC001594

Aparicio, F. L., M. Nieto-Cid, E. Borrull, E. Romero, C. A. Stedmon, M. M. Sala, J. M. Gasol, A. F. Ríos, and C. Marrasé. 2015. Microbially-mediated fluorescent organic matter transformations in the deep ocean. Do the chemical precursors matter? Front. Mar. Sci. **2**: 1–14. doi:10.3389/fmars.2015.00106

Arendt, K. E., M. D. Agersted, M. K. Sejr, and T. Juul-Pedersen. 2016. Glacial meltwater influences on plankton community structure and the importance of top-down control (of primary production) in a NE Greenland fjord. Estuar. Coast. Shelf Sci. **183**: 123–135. doi:10.1016/j.ecss.2016.08.026

Asmala, E., R. Autio, H. Kaartokallio, L. Pitkänen, C. A. Stedmon, and D. N. Thomas. 2013. Bioavailability of riverine dissolved organic matter in three Baltic Sea estuaries and the effect of catchment land use. Biogeosciences **10**: 6969–6986. doi:10.5194/bg-10-6969-2013

Baña, Z., B. Ayo, C. Marrasé, J. M. Gasol, and J. Iriberri. 2014. Changes in bacterial metabolism as a response to dissolved organic matter modification during protozoan grazing in coastal Cantabrian and Mediterranean waters. Environ. Microbiol. **16**: 498–511. doi:10.1111/1462-2920.12274

Bendtsen, J., J. Mortensen, and S. Rysgaard. 2014. Seasonal surface layer dynamics and sensitivity to runoff in a high Arctic fjord (Young Sound/Tyrolerfjord, 74°N). J. Geophys. Res. Oceans **119**: 6461–6478. doi:10.1002/2014JC010077

Bhatia, M. P., S. B. Das, K. Longnecker, M. A. Charette, and E. B. Kujawinski. 2010. Molecular characterization of dissolved organic matter associated with the Greenland ice sheet. Geochim. Cosmochim. Acta **74**: 3768–3784. doi:10.1016/j.gca.2010.03.035

Caporaso, J. G., C. L. Lauber, W. A. Walters, D. Berg-lyons, C. A. Lozupone, P. J. Turnbaugh, N. Fierer, and R. Knight. 2011. Global patterns of 16S rRNA diversity at a depth of millions of sequences per sample. Proc. Natl. Acad. Sci. USA **108**: 4516–4522. doi:10.1073/pnas.100008010

Catalá, T. S., and others. 2015. Turnover time of fluorescent dissolved organic matter in the dark global ocean. Nat. Commun. **6**: 5986.

Catalá, T. S., and others. 2016. Drivers of fluorescent dissolved organic matter in the global epipelagic ocean. Limnol. Oceanogr. **61**: 1–19. doi:10.1038/ncomms6986

Cauwet, G. 1999. Determination of dissolved organic carbon and nitrogen by high temperature combustion. *In* K. Grasshoff, K. Kremling, and M. Ehrhardt [eds.], Methods of seawater analysis. Wiley-VCH, p. 407–420.

Citterio, M., M. K. Sejr, P. L. Langen, R. H. Mottram, J. Abermann, S. H. Larsen, K. Skov, and M. Lund. 2017. Towards quantifying the glacial runoff signal in the freshwater input to Tyrolerfjord – Young Sound, NE Greenland. Ambio **46**: 146–159. doi:10.1007/s13280-016-0876-4

Coble, P. G. 1996. Characterization of marine and terrestrial DOM in seawater using excitation-emission matrix spectroscopy. Mar. Chem. **51**: 325–346. doi:10.1016/0304-4203(95)00062-3

Decelle, J., S. Romac, R. F. Stern, E. M. Bendif, A. Zingone, S. Audic, M. D. Guiry, L. Guillou, D. Tessier, F. Le Gall, P. Gourvil, A. L. Dos Santos, I. Probert, D. Vaulot, C. de Vargas, and R. Christen. 2015. PhytoREF: A reference database of the plastidial 16S rRNA gene of photosynthetic eukaryotes with curated taxonomy. Mol. Ecol. Resour. **15**: 1435–1445. doi:10.1111/1755-0998.12401

DeSantis, T. Z., P. Hugenholtz, N. Larsen, M. Rojas, E. L. Brodie, K. Keller, T. Huber, D. Dalevi, P. Hu, and G. L. Andersen. 2006. Greengenes, a chimera-checked 16S rRNA gene database and workbench compatible with ARB. Appl. Environ. Microbiol. **72**: 5069–5072. doi:10.1128/AEM.03006-05

Egge, J. K., and D. L. Aksnes. 1992. Silicate as regulating nutrient in phytoplankton competition. Mar. Ecol. Prog. Ser. **83**: 281–289. doi:10.3354/meps083281

Fellman, J. B., R. G. M. Spencer, P. J. Hernes, R. T. Edwards, D. V. D'Amore, and E. Hood. 2010. The impact of glacier runoff on the biodegradability and biochemical composition of terrigenous dissolved organic matter in near-shore marine ecosystems. Mar. Chem. **121**: 112–122. doi:10.1016/j.marchem.2010.03.009

Feng, X., J. E. Vonk, B. E. van Dongen, O. Gustafsson, I. P. Semiletov, O. V. Dudarev, Z. Wang, D. B. Montlucon, L. Wacker, and T. I. Eglinton. 2013. Differential mobilization of terrestrial carbon pools in Eurasian Arctic river basins. Proc. Natl. Acad. Sci. USA **110**: 14168–14173. doi:10.1073/pnas.1307031110

Fox, J., and S. Weisberg. 2011. An R companion to applied regression, 2nd ed. SAGE Publications, Inc.

Gonçalves-Araujo, R., M. A. Granskog, A. Bracher, K. Azetsu-Scott, P. A. Dodd, and C. A. Stedmon. 2016. Using fluorescent dissolved organic matter to trace and distinguish the origin of Arctic surface waters. Sci. Rep. **6**: 1–12. doi:10.1038/srep33978

Guillemette, F., and P. A. del Giorgio. 2012. Simultaneous consumption and production of fluorescent dissolved organic matter by lake bacterioplankton. Environ. Microbiol. **14**: 1432–1443. doi:10.1111/j.1462-2920.2012.02728.x

Hauptmann, A. L., T. N. Markussen, M. Stibal, and N. S. Olsen. 2016. Upstream freshwater and terrestrial sources are differentially reflected in the bacterial community structure along a small Arctic River and its estuary. Front. Microbiol. **7**: 1–16. doi:10.3389/fmicb.2016.01474

Holmes, R. M., A. Aminot, R. Kérouel, B. A. Hooker, and B. J. Peterson. 1999. A simple and precise method for measuring ammonium in marine and freshwater ecosystems. Can. J. Fish. Aquat. Sci. **56**: 1801–1808. doi:10.1139/f99-128

Holmes, R. M., J. W. McClelland, P. A. Raymond, B. B. Frazer, B. J. Peterson, and M. Stieglitz. 2008. Lability of DOC transported by Alaskan rivers to the Arctic Ocean. Geophys. Res. Lett. **35**: 3–7. doi:10.1029/2007GL032837

Hood, E., J. Fellman, R. G. M. Spencer, P. J. Hernes, R. Edwards, D. D'Amore, D. Scott, D. D. Amore, and D. Scott. 2009. Glaciers as a source of ancient and labile organic matter to the marine environment. Nature **462**: 1044–1047. doi:10.1038/nature08580

Jespersen, A.-M., and K. Christoffersen. 1987. Measurement of chlorophyll-a from phytoplankton using ethanol as extraction solvent. Arch. Hydrobiol. **109**: 445–454.

Jiao, N., G. J. Herndl, D. A. Hansell, R. Benner, G. Kattner, S. W. Wilhelm, D. L. Kirchman, M. G. Weinbauer, T. Luo, F. Chen, and F. Azam. 2010. Microbial production of recalcitrant dissolved organic matter: Long-term carbon storage

in the global ocean. Nat. Rev. Microbiol. **8**: 593–599. doi:10.1038/nrmicro2386

Jørgensen, L., C. A. Stedmon, T. Kragh, S. Markager, M. Middelboe, and M. Søndergaard. 2011. Global trends in the fluorescence characteristics and distribution of marine dissolved organic matter. Mar. Chem. **126**: 139–148. doi:10.1016/j.marchem.2011.05.002

Kjeldsen, K. K., N. J. Korsgaard, A. A. Bjørk, S. A. Khan, J. E. Box, S. Funder, N. K. Larsen, J. L. Bamber, W. Colgan, M. van den Broeke, M.-L. Siggaard-Andersen, C. Nuth, A. Schomacker, C. S. Andresen, E. Willerslev, and K. H. Kjær. 2015. Spatial and temporal distribution of mass loss from the Greenland ice sheet since AD 1900. Nat. Lett. **528**: 396–400. doi:10.1038/nature16183

Koroleff, F. 1983. Determination of nutrients, p. 125–187. *In* K. Grasshoff, M. Erhardt, and K. Kremling [eds.], Methods of seawater analysis. Verlag Chemie.

Kroon, A., J. Abermann, M. Bendixen, M. Lund, C. Sigsgaard, K. Skov, and B. U. Hansen. 2017. Deltas, freshwater discharge, and waves along the Young Sound, NE Greenland. Ambio **46**: 132–145. doi:10.1007/s13280-016-0869-3

Lawaetz, A. J., and C. A. Stedmon. 2009. Fluorescence intensity calibration using the Raman scatter peak of water. Appl. Spectrosc. **63**: 936–940. doi:10.1366/000370209778964548

Lawson, E. C., J. L. Wadham, M. Tranter, M. Stibal, G. P. Lis, C. E. H. Butler, J. Laybourn-Parry, P. Nienow, D. Chandler, and P. Dewsbury. 2014. Greenland Ice Sheet exports labile organic carbon to the Arctic oceans. Biogeosciences **11**: 4015–4028. doi:10.5194/bg-11-4015-2014

Lønborg, C., M. Middelboe, and C. P. D. Brussaard. 2013. Viral lysis of *Micromonas pusilla*: Impacts on dissolved organic matter production and composition. Biogeochemistry **116**: 231–240. doi:10.1007/s10533-013-9853-1

Lønborg, C., G. J. Herndl, and X. A. Alvarez-salgado. 2014. Production and degradation of fluorescent dissolved organic matter in surface waters of the eastern north Atlantic ocean. Deep-Sea Res. Part I Oceanogr. Res. Pap. **96**: 28–37.

Marie, D., C. P. D. Brussaard, R. Thyrhaug, G. Bratbak, and D. Vaulot. 1999. Enumeration of Marine Viruses in Culture and Natural Samples by Flow Cytometry. Appl. Environ. Microbiol. **65**: 45–52.

Meire, L., J. Mortensen, P. Meire, T. Juul-Pedersen, M. K. Sejr, S. Rysgaard, R. Nygaard, P. Huybrechts, and F. J. R. Meysman. 2017. Marine-terminating glaciers sustain high productivity in Greenland fjords. Glob. Chang. Biol. **23**: 5344–5357. doi:10.1111/gcb.13801

Middelbo, A. B., M. K. Sejr, K. E. Arendt, and E. F. Møller. 2018. Impact of glacial meltwater on spatiotemporal distribution of copepods and their grazing impact in Young Sound NE, Greenland. Limnol. Oceanogr. **63**: 322–336. doi:10.1002/lno.10633

Møller, E. F. 2007. Production of dissolved organic carbon by sloppy feeding in the copepods *Acartia tonsa*, *Centropages typicus*, and *Temora longicornis*. Limnol. Oceanogr. **52**: 79–84. doi:10.4319/lo.2007.52.1.0079

Møller, E. F., P. Thor, and T. G. Nielsen. 2003. Production of DOC by *Calanus finmarchicus*, *C. glacialis* and *C. hyperboreus* through sloppy feeding and leakage from fecal pellets. Mar. Ecol. Prog. Ser. **262**: 185–191. doi:10.3354/meps262185

Müller, O., L. Seuthe, G. Bratbak, and M. L. Paulsen. 2018. Bacterial response to permafrost derived organic matter input in an Arctic fjord. Front. Mar. Sci. **5**: 1–12. doi:10.3389/fmars.2018.00263

Murphy, J., and J. P. Riley. 1962. A modified single solution method for the determination of phosphate in natural waters. Anal. Chim. Acta **26**: 31–36.

Murphy, K. R., C. A. Stedmon, D. Graeber, and R. Bro. 2013. Fluorescence spectroscopy and multi-way techniques. PARAFAC. Anal. Methods **5**: 6557–6566. doi:10.1039/c3ay41160e

Murray, C., S. Markager, C. A. Stedmon, T. Juul-Pedersen, M. K. Sejr, and A. Bruhn. 2015. The influence of glacial melt water on bio-optical properties in two contrasting Greenlandic fjords. Estuar. Coast. Shelf Sci. **163**: 72–83. doi:10.1016/j.ecss.2015.05.041

Nagata, T., and D. L. Kirchman. 1992. Release of macromolecular organic complexes by heterotrophic marine flagellates. Mar. Ecol. Prog. Ser. **83**: 233–240. doi:10.3354/meps083233

Paulsen, M. L., H. Doré, L. Garczarek, L. Seuthe, O. Müller, R.-A. R. Sandaa, G. Bratbak, and A. Larsen. 2016. Synechococcus in the Atlantic Gateway to the Arctic Ocean. Front. Mar. Sci. **3**: 191. doi:10.3389/fmars.2016.00191

Paulsen, M. L., S. E. B. Nielsen, O. Müller, E. F. Møller, C. A. Stedmon, T. Juul-Pedersen, S. Markager, M. K. Sejr, A. Delgado Huertas, A. Larsen, and M. Middelboe. 2017. Carbon bioavailability in a high Arctic fjord influenced by glacial meltwater, NE Greenland. Front. Mar. Sci. **4**: 1–19. doi:10.3389/fmars.2017.00176

Poulet, S. A., R. Williams, D. V. P. Conway, and C. Videau. 1991. Co-occurrence of copepods and dissolved free amino acids in shelf sea waters. Mar. Biol. **108**: 373–385. doi:10.1007/BF01313646

Riemann, B., J. Fuhrman, and F. Azam. 1982. Bacterial secondary production in freshwater measured by (3)H-thymidine incorportion method. Microb. Ecol. **8**: 101–114. doi:10.1007/BF02010444

Rysgaard, S., T. G. Nielsen, and B. W. Hansen. 1999. Seasonal variation in nutrients, pelagic primary production and grazing in a high-Arctic coastal marine ecosystem, Young Sound, Northeast Greenland. Mar. Ecol. Prog. Ser. **179**: 13–25. doi:10.3354/meps179013

Sa, E. J. D., and H. Kim. 2017. Surface gradients in dissolved organic matter absorption and fluorescence properties along the New Zealand sector of the Southern Ocean. Front. Mar. Sci. **4**: 1–14. doi:10.3389/fmars.2017.00021

Sanders, R., D. Caron, and U. G. Berninger. 1992. Relationships between bacteria and heterotrophic nanoplankton in marine and fresh waters: An inter-ecosystem comparison. Mar. Ecol. Prog. Ser. **86**: 1–14. doi:10.3354/meps086001

Schlitzer, R. 2016. Ocean data view; [accessed 2017 September 01]. Available from http://odv.awi.de

Schneider-Zapp, K., M. E. Salter, P. J. Mann, and R. C. Upstill-Goddard. 2013. Technical note: Comparison of storage strategies of sea surface microlayer samples. Biogeosciences **10**: 4927–4936. doi:10.5194/bg-10-4927-2013

Sejr, M. K., C. A. Stedmon, J. Bendtsen, J. Abermann, T. Juul-Pedersen, J. Mortensen, and S. Rysgaard. 2017. Evidence of local and regional freshening of Northeast Greenland coastal waters. Sci. Rep. **7**: 13183. doi:10.1038/s41598-017-10610-9

Sipler, R. E., C. T. E. Kellogg, T. L. Connelly, Q. N. Roberts, P. L. Yager, and D. A. Bronk. 2017. Microbial community response to terrestrially derived dissolved organic matter in the coastal Arctic. Front. Microbiol. **8**: 1–19. doi:10.3389/fmicb.2017.01018

Søndergaard, M., and M. Middelboe. 1995. A cross-system analysis of labile dissolved organic carbon. Mar. Ecol. Prog. Ser. **118**: 283–294. doi:10.3354/meps118283

Sosa, O. A., S. M. Gifford, D. J. Repeta, and E. F. Delong. 2015. High molecular weight dissolved organic matter enrichment selects for methylotrophs in dilution to extinction cultures. ISME J. **9**: 2725–2739. doi:10.1038/ismej.2015.68

Stedmon, C. A., and R. M. Cory. 2014. Biological origins and fate of fluorescent dissolved organic matter in aquatic environments, p. 278–300. *In* P. Coble, J. Lead, A. Baker, D. M. Reynolds, and R. G. M. Spencer [eds.], Aquatic organic matter fluorescence. Cambridge Univ. Press.

Stedmon, C. A., and N. B. Nelson. 2015. The optical properties of DOM in the ocean, 2nd ed. Elsevier.

ter Braak, C., and P. Šmilauer. 2012. Canoco Reference Manual and User's Guide: Software for Ordination, Version 5.0 t.

Urban-Rich, J., J. T. McCarty, and M. Shailer. 2004. Effects of food concentration and diet on chromophoric dissolved organic matter accumulation and fluorescent composition during grazing experiments with the copepod *Calanus finmarchicus*. ICES J. Mar. Sci. **61**: 542–551. doi:10.1016/j.icesjms.2004.03.024

Walker, S. A., R. M. W. Amon, and C. A. Stedmon. 2013. Variations in high-latitude riverine fluorescent dissolved organic matter: A comparison of large Arctic rivers. J. Geophys. Res. Biogeosci. **118**: 1689–1702. doi:10.1002/2013JG002320

Ward, C. P., R. L. Sleighter, P. G. Hatcher, and R. M. Cory. 2014. Insights into the complete and partial photooxidation of black carbon in surface waters. Environ. Sci. Process. Impacts **16**: 721–731. doi:10.1039/C3EM00597F

Wilson, B., O. Müller, E. -L. Nordmann, L. Seuthe, G. Bratbak, and L. øvreås. 2017. Changes in Marine Prokaryote Composition with Season and Depth Over an Arctic Polar Year. Front. Mar. Sci. **4**: 1–17.

Wood, E. D., F. A. J. Armstrong, and F. A. Rich. 1967. Determination of nitrate in seawater by cadmium-copper reduction to nitrate. J. Mar. Biol. Assoc. U. K. **47**: 23–31.

Wünsch, U. J., K. R. Murphy, and C. A. Stedmon. 2015. Fluorescence quantum yields of natural organic matter and organic compounds : Implications for the fluorescence-based interpretation of organic matter composition. Front. Mar. Sci. **2**: 1–15. doi:10.3389/fmars.2015.00098

Yamashita, Y., and E. Tanoue. 2008. Production of bio-refractory fluorescent dissolved organic matter in the ocean interior. Nat. Geosci. **1**: 579–582. doi:10.1038/ngeo279

Zubkov, M. V., P. H. Burkill, and J. N. Topping. 2007. Flow cytometric enumeration of DNA-stained oceanic planktonic protists. J. Plankton Res. **29**: 79–86. doi:10.1093/plankt/fbl059

Conflict of Interest

None declared.